Feasibility Analysis for Electrically-Powered Hoverboard

A Senior Project
presented to
the Faculty of the Aerospace Engineering Department
California Polytechnic State University, San Luis Obispo

In Partial Fulfillment
of the Requirements for the Degree
Bachelor of Science

By

Cameron Chan, Jason Cortez, and Jay Lopez

March, 2012

Feasibility Analysis for Electrically-Powered Hoverboard

[Senior Project]

Cameron Chan[1], Jason Cortez[1] and Jay Lopez[1]
California Polytechnic State University
Aerospace Engineering Department, San Luis Obispo, CA, 93407

[1] Aerospace Engineering Undergrad, Aerospace Engineering, 1 Grand Ave., San Luis Obispo, CA 93407

Abstract

Composite materials are engineered by combining two or more constituent materials with significantly different physical or chemical properties in such a way that the constituents are still distinguishable, and not fully blended. Due to today's high rising prices of gasoline and aviation fuel costs, many manufacturers have turned to the use of lightweight composites in their designs due to the advantages of the composite material, which include outstanding strength, excellent durability, high heat resistance, and significant weight reduction that the composite material properties hold. The purpose of this project is to design and construct a composite structure for an electrically-powered hover board designed for human flight. The hover board composite structure consists of three sandwich composite I-beams as the base of the structure where both the flanges and web are composed of fiberglass and a type of foam as the core. The three composite I-beams is essential to our design because as beam theory states, the I-shaped section is a very efficient form for carrying both the bending and shear loads in the plane of the web, which are the two main types of loads that we will encounter. The goals of the system are as follows: 1) the structure of the hover board will be able to withstand all forces and moments created by propulsion system and person; 2) the propulsion system will produce enough thrust to accommodate vertical takeoff for a 170 lb person and achieve a minimum height of three inches; 3) creating a new segment in the aviation and recreational vehicle markets. The goals of this project are very important to achieve as the hover board will be the first of its kind that uses a propulsion system without implementing a skirt. This means that all lift will be created by the four ducted fans in our propulsion system. Once the hover board has been optimized and finalized, it will expand the market of commercially available VTOL systems. At first this technology can be utilized for merely recreation but as time progresses the technology can be expanded to industry. It will replace currently existing cargo movement systems such as forklifts.

Nomenclature

A	=	extensional stiffness coupling
B	=	bending extension coupling stiffness
D	=	maximum deflection of the center of the beam
E	=	Young's modulus
$\overline{EA}$	=	equivalent axial stiffness of entire cross section
F	=	force
G	=	shear modulus
L	=	support span
M	=	resultant laminate moment
N	=	resultant laminate force
Q	=	reduced stiffness matrix
P	=	load at a given point on the load deflection curve, and d refers to the depth of the beam
R	=	rate of crosshead motion
S	=	maximum stress in the outer fibers occurs between the two central loading points
T	=	transformation matrix
V	=	velocity
Z	=	rate of straining of the outer fibers
b	=	width of the beam
d	=	depth of the beam
h	=	height of beam
r	=	maximum strain in the outer fibers
z	=	incremental thickness
$\propto$	=	angular orientation of laminae
γ	=	shear strain
ε	=	strain
ν	=	Poisson's ratio

ρ = density
σ = stress
τ = shear stress
θ = angle of rotation

superscripts
‘ = transpose
subscripts
1 = primary horizontal axis
2 = primary vertical axis
f1 = top flange of box beam
f2 = bottom flange of box beam
fl = top or bottom flange of box beam
k = k^{th} layer
lw = left web
rw = right web
sl = particular sub-laminate of box beam

Introduction

The traditional idea of a hovering vehicle typically calls for a design that implements a skirted feature onto the craft. The basic principle of this design incorporates a fan that blows low velocity-high pressure air into a bag to create a cushion of air for the vehicle to rest on.[1] This cushion of air allows the vehicle to traverse a variety of terrain with the same level of ease. Historically, various hovercrafts have been designed with moderate to good success. The first successful attempt of developing this type of vehicle was achieved in the late 1930s by a Finish aeronautical engineer. Since then, several modifications have been applied to the original design to improve efficiency and effectiveness. Significant improvements mainly center on the skirt aspect of the vehicle. Although the skirt is very effective in providing vertical thrust, the notion of creating a personal hovering vehicle without the use of a skirt is ideal. The portable characteristics of skateboard would provide the most convenience for a personal vehicle. On another note, the technology behind a hovercraft would allow the vehicle to be flexible in navigating different types of terrain. Marrying these two ideas into one concept results in the idea of a hover board—a mode of transportation that is robust and convenient for storage. In order to achieve these goals, the board must address the issues of providing substantial lift for an average person’s weight without the need of big and heavy components. A solution that remedies this problem is designing a structural core that is light and strong. This structural base must be able to handle the load of a 160 lb individual as well as the loads created by the lifting forces of the vehicle. As a result, carbon fiber is a prospective material being investigated for the structural base of the hover board.

Figure 1: The traditional style hover craft implements a skirted feature.[2]

Carbon fiber provides an excellent strength-to-weight ratio for many structural components.[3] The manufacturability of the material also allows for custom strength to be built into a variety of shapes for practically any structural design. Using carbon fiber in the structure of the hover board would substantially reduce the weight of the vehicle to allow a feasible design that can incorporate smaller lifting components at a lesser cost. However, the issue at hand is determining the amount of carbon fiber material than can withstand the corresponding loads without

overdesigning the structure and increasing manufacturing costs. Devising the major structural components to handle the loads and the specific methods for determining the right configuration of the fibers' direction over several layers are the first steps in analyzing the required material for the design.

The composites being used today for airframes are considered advanced composite materials, which is the type of materials that will be applied to the hover board.[5] Advanced composites consist of high modulus, continuous fibers like carbon and boron and an essentially homogenous matrix.[5] A basic example of a composite material is fiberglass, which uses glass fibers and an epoxy resin to create a high strength composite used in everyday applications. Composite fibers are primarily used as reinforcement to the surrounding matrix. Generally, reinforcement fibers consist of three types: organic fibers, ceramic fibers, and metallic fibers. Organic fibers offer high strengths for very light weights (i.e. glass, graphite carbon, etc.). Ceramic fibers are used when the material needs to withstand high temperatures and insulate against heat. Examples of ceramic fibers are quartz, silicon carbide, alumina, etc. Lastly, metallic fibers allow the composite to conduct or dissipate heat and electricity.

Figure 2: The Boeing 787 Dreamliner commercial aircraft takes advantage of the advanced composite materials[4]

In addition to the fiber structure, the composite material requires a matrix to hold the fibers in place. The matrix is perhaps the most important part of the composite material because it not only keeps the fibers in the desired location, but it also protects the fibers from moisture and chemical corrosion. This can lead to embrittlement and premature failure. It is important to keep the fibers in the designed origin because they will be able to more effectively bear the applied loads.[3] Furthermore, the matrix also resists against crack propagation and provides all the interlaminar shear strength of the composite. Ultimately, the matrix decides many important design parameters for the composite. For example, the matrix type determines the compressive strength, shear, operating temperature and the fabrication process.

Matrices are either made from organic or non-organic materials. Organic matrices are split up into two categories: thermoset and thermoplastic. Thermoset matrices have recently been dominating the composite market because of their versatility. Most importantly, thermoset matrix based composites can be formed into complex shapes while still providing very high strengths. Thermoset composites are used in airframe design for primary structures. A thermoset matrix has many distinct properties. During the long curing process the thermoset undergoes a chemical change, making the process irreversible. Additionally, thermosets have low viscosity and a tacky pre-preg. The advantages to using a thermoset are their low processing temperature, low viscosity, good fiber wetting, and complex shaping. In contrast, the long processing time, restricted storage and required refrigeration all hinder the use of thermosets. Types of thermosets used in airframe design are epoxies, polyester, phenolics, bismaleimide, and polymides.[3] The epoxy family is the most widely used thermoset matrix system in the advanced composite field, but it's low resistance to high temperature variations restricts the use in aerospace applications, where high service temperatures are required. Epoxy matrices are most useful for use with glass, carbon/graphite, boron, and aramid. Currently, the development of more advanced epoxies is being done to accommodate increasing requirements. Epoxies that have been unmodified are usually brittle and modification is necessary to increase its damage resistance, which results in a toughened epoxies. The versatility of epoxy is advantageous; however, environmental hazards can have detrimental effects on the matrix such as: temperature, moisture, fuel, cleaning agents, and ultraviolet light. These hazards completely eliminate the demand to use epoxy on external aircraft pieces.

If the composite structure is in need of a more flexible organic matrix, thermoplastics may be the type to choose. Thermoplastics are non-reacting (meaning no curing), can be reprocessed, are high viscosity, and have the ability to endure short processing times. Furthermore, thermoplastics come with the advantages of having superior toughness, reusable excess, reformable parts, rapid (low cost processing), infinite shelf life, and high delamination

resistance. The disadvantages to thermoplastics consist of a high processing temperature requirement, a smaller resistance to chemical solvents, a limit in the amount of processing experience, and a small database.[5] Generally, thermoplastic composites have been used for non-structural airframe components.[3]

Non-organic matrices (metals, carbon, and ceramic materials), have not seen much progression in the past years because of their high costs and limited applications. Types of metal matrices are aluminum, titanium, magnesium, and copper. All metal matrices have high fracture resistance. Carbon matrix structures (carbon/carbon) are often used in areas subjected to very high temperatures such as aircraft breaks, rocket nozzles, rocket nose cones, and jet engine turbine wheels. Remarkably, the strength of the composite increases as the temperature rises. Ceramic composites are generally characterized as having high melting points, high compressive strength, and excellent resistance to oxidation. Like carbon/carbon composites, ceramic composites are also used for aircraft brakes. Another advantage to ceramics is their ability to be made from performs which reduce the amount of post-machining necessary to complete the part. However, ceramics are susceptible to moderate tension, impacts and thermal shocks.[3]

Once the designer has chosen a composite, the next step is to choose the type of material form to use. Material forms are divided into two subgroups: staple and continuous. The staple orientation includes random orientation or preferred orientation. Continuous forms include unit-tapes, woven fabrics, pre-forms, etc. Figure (2) shows an example of a sheet of woven carbon fiber. Most forms can be obtained either dry or pre-impregnated with the desired matrix. Dry forms require some method of applying matrix during the lay-up process, whereas the pre-preg forms require no additional matrix application. Uni-tape forms are advantageous in that they have flexibility in design and maximum structural properties; however, they have poor drapability and can lead to possible fiber misalignment. Woven fabrics provide good drapability and are least costly in the lay-up cost. The disadvantages to woven fabrics are that there are losses in properties due to crimping in the fiber and are less flexible in design. Pre-plied fabrics and stitched fabrics are similar in that they have reduced lay-up costs while having a loss in design flexibility. Furthermore, they allow for resin injection molding and provide exceptional fiber stability needed for pultrusion. Unidirectional fabrics, as tested in the experiment and as shown in Fig. 2, provide improved drapability, fiber alignment, and minimal reductions in fiber strength. With only one disadvantage for unidirectional fibers, having a slight weight penalty, the variety of advantages outweighs the one disadvantage and lead to a great form.

Figure 3: Unidirectional carbon fiber is just one of the many types of composite forms.[6]

In addition to knowing the types of composite materials and forms, the fabrication process types are also important to note. All composite manufacturing follows the same general process plus or minus a few steps depending on the type of composite. Regardless, the process starts with material selection and material batch acceptance. Then the composite is laid up based on the type of composite. The lay-up process can be broken up into three types: Wet lay-up, draw, and pre-preg. Wet lay-up is a method where the reinforced product is made by introducing the matrix as a liquid to the reinforcing fibers. The draw lay-up method uses a vacuum to distribute the liquid matrix throughout the fibers; thus, increasing the likelihood of the matrix being more evenly distributed. Last, pre-preg lay-ups come ready to be molded and cured. Pre-preg composite materials are great for basic projects and batch testing; however, they create a storage problem, as they must be kept in a freezer.[3]

Furthermore, it is pertinent to understand the concept of a composite laminate. A laminate is a bonded stack of laminae, where the fibers can be oriented symmetrically about the middle surface or anti-symmetrically about the middle surface of the laminate. The purpose of lamination is to tailor the directional dependence of strength and stiffness of a composite material to match the loading environment of the structural element. Laminates are suitable for this purpose because the principal material directions of each layer can be oriented according to need. For example, to obtain an extensional stiffness far higher in one direction than the other, half of the layers in a laminate would be oriented in a ninety degree direction from the other half of the layers in the laminate. Symmetry about the middle surface of a laminate is often desirable to avoid coupling between bending and extension.[5] In order to achieve particular design requirements, the use of unsymmetrical laminates is necessary. This is true especially for a form of coupling necessary to make jet turbine fan blades with pre-twist without the use of a complex mold. Anti-symmetric laminates must have an even number of layers if adjacent laminae also have altering signs of the principal material property directions with respect to the laminate axes. If the adjacent laminae do not have altering signs, this is not necessary and the number of layers does not have to be even. A common type of an anti-symmetric laminate is a cross-ply anti-symmetric laminate which consists of an even number of orthotropic laminae laid on each other with principal material directions alternating at zero degrees and ninety degrees to the laminate axes. A more complicated cross-ply laminate is one where the adjacent layers do not always have an alternating sequence of zero and ninety degrees. A regular anti-symmetric angle ply laminate has all laminae with equal thickness and is common because of the simplicity of fabrication. As the number of layers increases, the coupling stiffness will approach zero. A less common type of an anti-symmetric laminate is that of an angle-ply laminate. This type has laminae oriented at +α degrees to the laminate coordinate axes on one side of the middle surface and the corresponding equal-thickness laminae oriented at –α degrees on the other side at the same distance from the middle surface. A more complicate version will include mixed materials with mixed lamination angles. A regular anti-symmetric angle-ply laminate has laminae all of the same material and thickness for ease of fabrication. As the number of layers in the laminate increases the bending-extension coupling stiffnesses will approach zero. Overall, asymmetric laminates are the more general class of laminate, where lack of symmetry often occurs by design as in deliberately constructing a non symmetric laminate. Further, often symmetric laminates subjected in service to heating from one side so that the resulting thermal gradient acting on the temperature dependent material properties renders the laminate unsymmetric.[8]

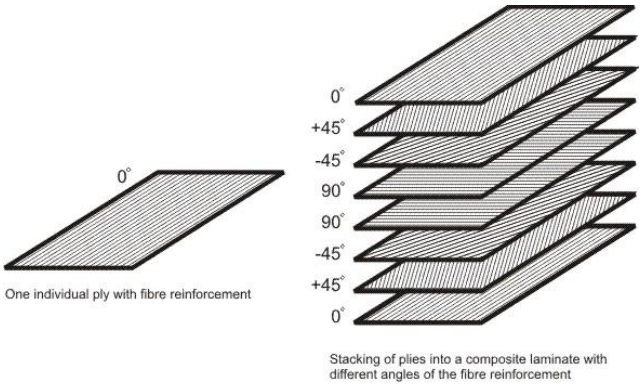

Figure 4: This figure shows a symmetrical laminate plate, which is desired to avoid coupling between bending and extension.[7]

The hover board's internal structural configuration is comprised of two composite boxed beams spanning the length of the vehicle that attach to a pair of ducted fans at each end of the board while a lightweight skin material encases all structural members. Boxed beams are known for efficiently withstanding bending and shearing loads because of its cross-sectional shape that allows for minimal material needed to withstand a load that a solid rectangular shape can endure. Creating a boxed beam out of composite material would reduce the weight of the beam even further. For added structural rigidity and performance,

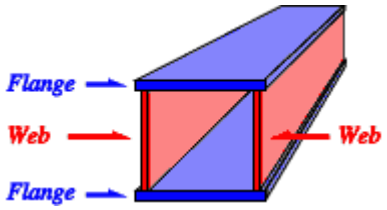

Figure 5: Boxed beams are efficient in withstanding bending and shearing loads because of the cross-sectional shape.[9]

implementing a foam core into the beam is investigated for optimum results. Consequently, the composite boxed beam is primarily constructed using four composite sandwich materials that make up the two flanges and two webs for each boxed beam. Each composite sandwich material consists of two laminate plates and a core.

To best visualize the structure of a sandwich core panel it is best to use the analogy of a simple I-beam. The sandwich core panel is analogous to an I-beam as the laminate plates act as the flanges and the core acts as the web of the panel. The laminate plates are subject to tension/compression and are a large responsibility for the strength of the sandwich. The core's primary job is to support the skins so that they do not buckle or deform, staying fixed relative to each other. The core experience mostly shear stresses as well as a small amount of vertical tension and compression. The core's material properties and thickness is extremely important for the sandwich panel, as it will determine the stiffness of the panel. Unlike the simple beam, which is designed to withstand the stresses most likely along the x axis and bending about the y axis, the sandwich panel can be stresses along about any axis lying in the x-y plane. No reinforcing elements are needed because they are already built into the structure.[10]

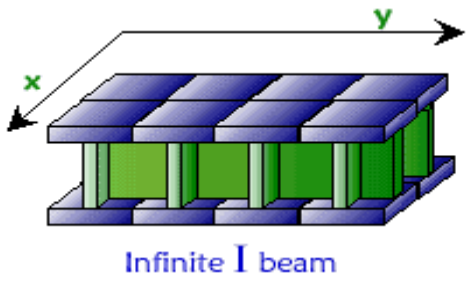

Figure 6: The composite sandwich panel is analogous to an I-beam.[11]

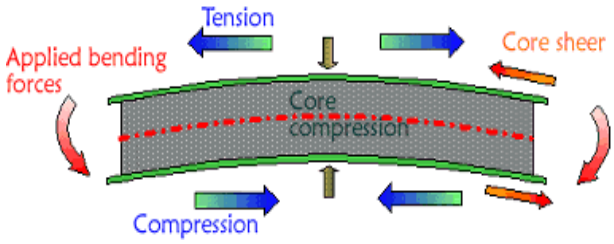

Figure 7: The strength of the composite sandwich panel, like the I beam mostly comes from the laminated plates(flanges) bonded to each side of the core.[11]

In order to measure the characteristics and behavior of a material, such as a composite material, scientists and engineers will apply a variety of materials testing. The data that is obtained from the materials testing can then be used in determining the material safety level, durability, and how long the material will be able to last under normal wear and tear. The analysis of the material data will then lead to the suitability of a material for various applications, such as a building or aircraft construction. Materials testing can be broken down into 5 major categories which include: mechanical testing, testing for corrosion, radiation, biological deterioration, and nondestructive testing. For our experiment we will only be concentrating on the static tests portion of mechanical testing. The static tests consist of static tension and compression tests and static shear and bending tests. A simple static tension test determines the breaking point of the material and its elongation, designated as strain. A static tension test requires a test piece, a test machine that applies, measures, and records various loads, and an appropriate set of grips to grasp the test piece. Static compression tests determine a material's response to crushing, or support type loading. The testing machine and extensometer are very similar to the tensile tests. A disadvantage of the compression test is the possibility that the sample or load chain may buckle prior to the material failure. To prevent this type of buckling, the test specimens should be kept short and stubby. Static shear tests indicate the amount of deformation response of a material when forces are being applied tangentially. These tests are applied primarily to thin sheet materials, either metals or composites, such as fiberglass reinforced plastic. Due to tensile testing being very difficult to perform directly upon certain brittle materials, such as glass and ceramics, the tensile strength can

also be measure by applying bending tests, in which tensile stresses develop on one side of the bent member and corresponding compressive stresses develop on the opposite side. If the material is substantially stronger in compression than tension, failure initiates on the tensile side of the member and, hence, provides the required information on the material tensile strength. Due to the necessity to know the exact magnitude the tensile stress at failure in order to establish the strength of the material, the bending method is only applicable to a very restricted class of materials and conditions. Types of bending tests include three and four point bending.

Three point bend testing provides values for modulus of elasticity in bending, flexural stress, flexural strain, and the flexural stress-strain response of the material. The main advantage of the three point bend test is the ease of the specimen preparation and testing. However the disadvantage is that the results of the testing method are sensitive to specimen and loading geometry and strain rate. Three point bending tests consist of two parallel supports for the sample and a single loading pin in the middle, between the supports, where the force is introduced. The support pins must be mounted in such a way that they can rotate freely on their axis in order to minimize the influence of friction on the measurement. One of the supports must also be able to rotate about an axis perpendicular to this and parallel to the axes of the sample so that the test piece can align itself when under stress. The loading pin must also possess similar rotational axes in order to ensure the uniform application of force on the test piece. The force is introduced perpendicularly to the test piece plane and/or the support plane. The typical setup for three-point bending testing can be seen in Fig. 8. Four point bend testing is very similar to the three point bend test, but instead of just one loading pin acting in the middle, there are two loading pins, whose centers are separated by half of the distance between the supports. It must be noted that for all testing, the American Society for Testing and Materials (ASTM) guidelines must be followed.[12]

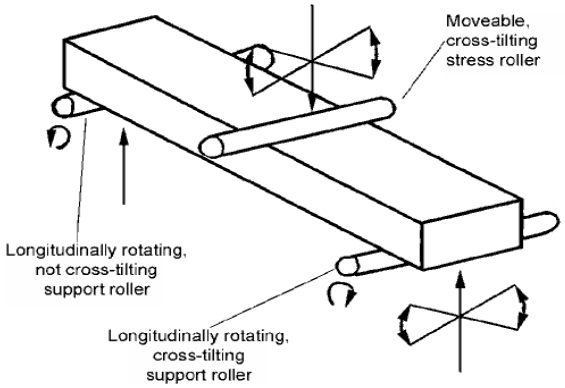

Figure 8: This figure shows the schematic of the three-point bending testing.[13]

Due to the nature of the design, the hover board's structure is expected to endure a 4-point bending load across the length to the beam. However, in order to include the worst case scenario, a concentrated load in the middle of the boxed beam, a 3-point bending load is also applied. These three point loads are deducted from the weight of a person standing is in the middle of the hover board and the pair of lifting forces applied vertically up at each ends of the beams where the fans are located. In order to investigate the structural properties of the beam, a 3-point bending test is conducted on several small specimens in different axes of the beam, such as testing the sandwich panel vertically and horizontally. Along with testing for worst case scenario, the 4-point bending was also applied to our test specimens for both the vertical case and the horizontal test case. The 4-point bending test is a more realistic test for the hover board due to the balanced load that the rider will create standing in a widened stance. After obtaining important information from the test such as the material's modulus of elasticity, bigger specimens are created to investigate the structural performance expected of such beams for a hover board design.

Important data investigated is the deflection of the beams under the given test and the stresses on the structure. The strain and stress determined in the beams from the experiment would then allow for optimization of the structure. From this analysis, the design of the hover board's structure is modified until the required configuration is obtained to effectively carry out the function of vehicle.

Apparatus and Procedures

In order to begin the design and fabrication process of the hover board project, the first thing that had to be determined was the internal structure of the hover board. The reason that the internal structure of the hover board is the most critical part of the design is because the internal structure bears all of the loads acting on the hover board. For this reason, we carefully analyzed all forces that would be acting on the hover board and carefully looked at the incorporation of the I-beam and boxed beam. Due to the large amounts of bending and torsion, we found that the integration of two composite boxed beams for our internal structure would be feasible, providing a very high structural integrity. The inclusion of the boxed beam was chosen instead of the I-beam because boxed beams can resist a bigger torsion load and can also carry higher bending loads than an I-beam of equal height due to the multiple vertical webs. However, with the boxed beam, there is added weight with the inclusion of the extra vertical web, and analysis was conducted on this added weight to conclude if the added vertical web was a necessity to the design. By using the densities of the composite materials, it was concluded that the structural integrity of the boxed beams far outweighed the additional weight added to the system.

Once the internal structure of the hover board was known, it then had to be determined the type of composite material would be implemented for the boxed beams and the number of plys the composite sandwich webs and flanges would need to consist of for strength purposes. The types of composite materials that were considered were expired pre-preg fiberglass, expired pre-preg carbon fiber, and non-expired pre-preg carbon fiber. . To obtain each of the materials mechanical properties, multiple mechanical tests were configured on the Instron machine.

Figure 9: All mechanical testing was done on the Instron 8800 servohydraulic fatigue testing machine.[14]

In order to perform testing on the Instron machine, the lay-up of the composite sandwich beams first needed to be accomplished. The first step in assembling the composite sandwich beams was to cut up the composite sheets and core into equal sized pieces, which was chose to be 1ft by 1ft. The number of composite sheets varied for each composite sandwich beam, to find a healthy balance between structural strength and weight that could be applied to the hover board. For example, if a two ply composite sandwich beam were to be tested, then a total of four composite sheets would be needed along with the core material. After the composite sheets and core were cut into equal sized pieces, the manufacturing process of the composite sandwich was then ready to begin.

When choosing a manufacturing process for the composite sandwich beam, it was made sure that the process that was chosen would be adept to the hover board. With the dimensions of the hover board being very large, there was a limited amount of manufacturing processes to choose from as the hover board was too big for Cal Poly's Structures Lab autoclave. For this reason, we chose to do a hand lay-up of the composite sandwich along with a vacuum bag molding. To perform the hand lay-up for the expired pre-preg composite sheets, a two-part resin was applied, which consisted of epoxy and hardener. However, because of the expired pre-preg that was already applied to the composite sheet, it was made sure that a lot of resin was applied to each sheet to make sure that a good bond would exist between each composite sheet. To create a good bond between the core and the laminates, a lot of resin was applied. Creating a good bond between the core and laminates were extremely important because the expected first type of failure that was believed to occur when using three-point bending for a composite sandwich beam is delamination of the core and laminate as seen in Fig. 9.

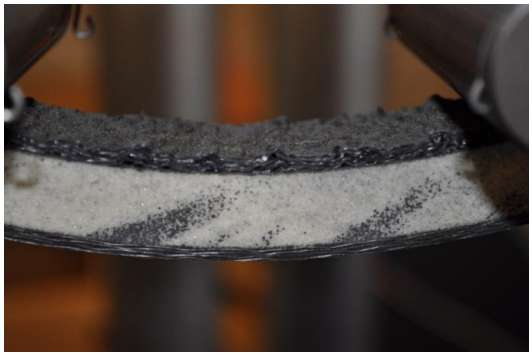

Figure 9: Creating a good bond between the core and laminates is very important because the first expected type of failure is delamination and buckling.

Once the hand lay-up was complete the composite sandwich beam was then prepared for vacuum bag molding. The reason that the vacuum bag molding was used was because vacuum bag molding is a room temperature cure and as mentioned before the hover board is too big for any composite curing machine at Cal Poly's Structures Lab. To perform the vacuum bag molding, two pieces of nylon bagging film were cut slightly larger than the composite sandwich sheet. The

composite sandwich sheet is then placed on top of one of the nylon bagging film pieces. Once the composite sandwich is placed on the nylon bagging film, sealant tape is applied to the outer portion of that nylon bagging film. After sealant tape is applied to the outer portion of the first nylon bagging film, the second nylon bagging film was then placed on top of the bottom one sealing the two pieces together. However, the bottom portion of the two pieces should be left open until the vacuum bag tubing is carefully secured. After tubing is secured and the bag is checked to make sure everything is sealed with no leaks, the vacuum is then ready to be turned on and the composite sandwich sheet will be cured in an 8 hour process. However, it should be noted that the longer the composite is cured, the stronger the composite material will be.

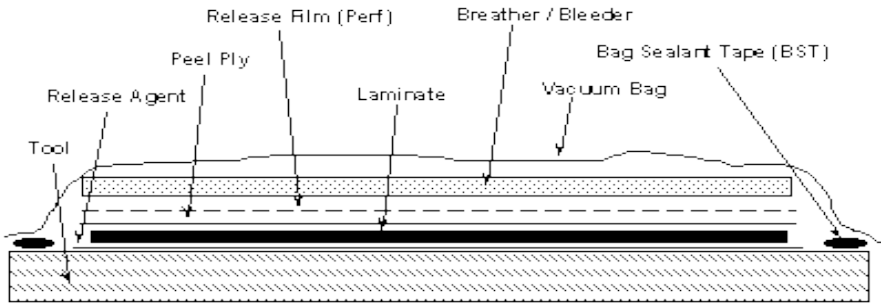

Figure 10: This figure shows how a composite laminate or composite sandwich panel should be prepared to cure the composite using the vacuum bag molding manufacturing process.[15]

After the curing process is complete, the composite sandwich sheet is then ready to be transformed in to test pieces. These test pieces should conform to ASTM standards, as for 3 point bending there should be a 16:1 ratio between the length of the test piece and the height of the test piece. To cut the composite sandwich sheet into ASTM standardized test pieces, a tile saw is used.

After the dimensions of the test pieces were up to standard, the test pieces were then ready for mechanical testing using the Instron machine. The mechanical tests that have been chosen to be performed on the composite sandwich beam test pieces were three point bending and four point bending as seen in Fig. 11 and Fig. 12.

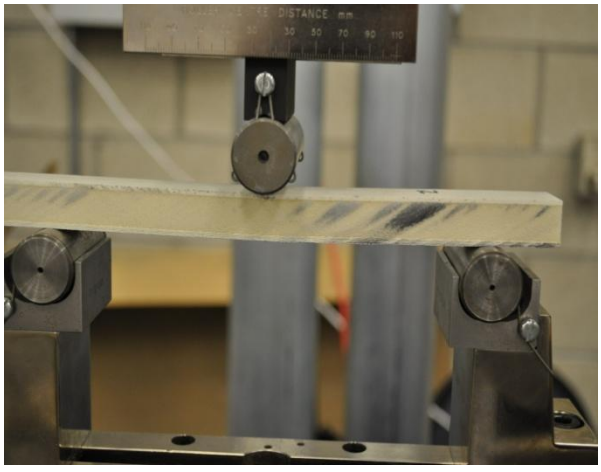

Figure 11: This figure shows a fiberglass composite sandwich panel in 3-point bending, which is tested for the worst case scenario of our hover board.

Figure 12: This figure shows a carbon fiber composite sandwich panel in 4-point bending, which is the more realistic type of testing for the hover board.

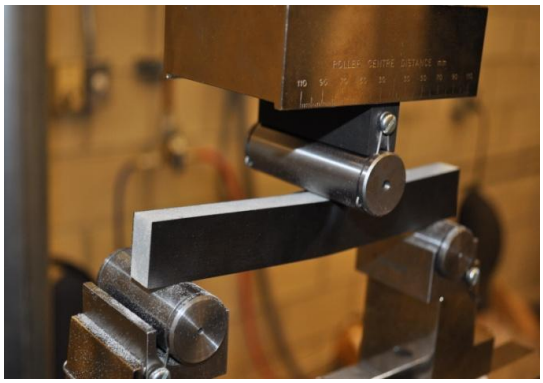

Figure 13: The composite sandwich panels were also tested on its side to model the webs of the boxed

The reason that three point and four point bending is chosen is because a free body diagram of the system will show simple supports on both edges of the beam with a distributed force in the middle of the beam. So to account for the worst case scenario, three point bending is used to illustrate a concentrated load. However, the four point bending is the more realistic case that the hover board will ever face as the load in the middle of the hover board will be coming from a person in a widened stance across the middle section of the hover board. Before the beam can be tested, the rate of the cross head motion must be changed in order to comply with ASTM standards. The rate of the cross head motion can be changed manually by entering the setting tabs of the Bluehill software. For all three composite materials, composite sandwich beams were tested using three and four point bending both vertically and horizontally as seen in Fig. 12. All data was recorded using the Bluehill software in the computer, computing a stress vs. strain curve.

Once all of the mechanical testing is done for the different lay-ups of the composite materials and number of plys, the data is analyzed to conclude which configuration of the composite sandwich would be best to implement into the design of the hover board. To manufacture the internal structure of the hover board (composite boxed beams), the aid of the aerospace company, C&D Zodiac was used to ease the process. C&D Zodiac was able to streamline the manufacturing process by donating pre-constructed flat panels (composite sandwiches) with the desired configuration and also allowing the use of their tools, such as the three-axis cutting machine. In order to use the three axis cutting machine, a Solid model drawing is constructed with the use of finger joints and slip joints to program the machine to make the exact pieces needed to construct the hover board. The addition of the finger joints and slip joints will allow the structure of the hover board to be put together like a jig-saw puzzle, as seen in figure blah. Once the pieces are cut to exact dimensions with the addition of finger joints and slip joints, all of the pieces are combined and the joints are bonded together using a suitable adhesive, such as epoxy. The internal structure of the hover board is then clamped to secure the joints until the adhesive cure is complete. In order to reduce weight and have a clean finish, any excessive adhesive is then sanded down to create a nice smooth finish.

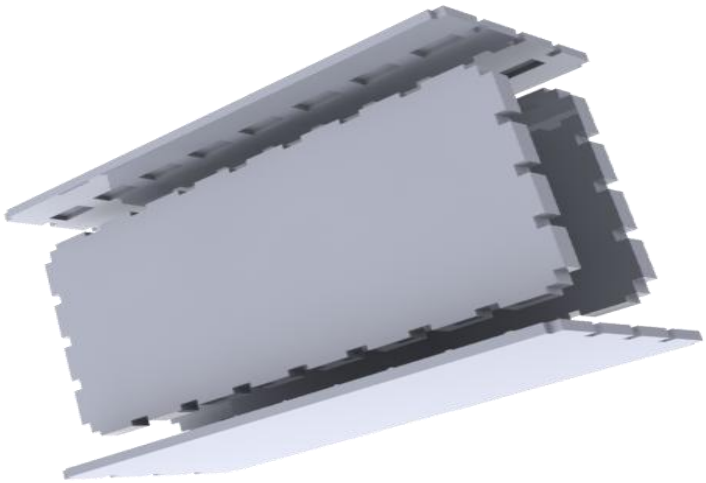

Figure 14: The use of finger joints will be implemented onto the hover board design. This figure shows the exploded view of the boxed beam with the finger joints shown.

After the internal structure is built, the nacelles and the fan blades are constructed, which will be used to create the thrust needed for the hover board to achieve vertical take-off. To assemble the nacelles and fan blades out of composites in the most efficient way possible, the resin transfer molding manufacturing process was implemented. Resin transfer molding is used to mold components with complex shapes, large surface areas, and provides a smooth finish to both sides of the composite material. To perform the resin transfer molding, a fixed closed mold cavity is made for both the nacelles and the fan blades. Once the closed mold cavity is built, a thermosetting resin is then injected into the cavity. The resin then wets through the reinforcement and solidifies to form into a composite part. The nacelle will consists of two symmetrical parts, which will then be bonded together with the use of finger joints to construct the full nacelle. The fan blades will be constructed by using one molded tool and not by parts. The nacelles and the fan blades require great precision because of the requirements to produce thrust with the fan blade and nacelle.

Figure 15: The nacelle will consist of two symmetrical parts, which will then be bonded by finger joints to complete the whole nacelle duct.[16]

Theoretical Analysis

Classical laminate theory is an extension of the theory for bending of homogeneous plates, but with an allowance for in-plane tractions in addition to bending moments, and for the varying stiffness of each ply in the analysis. The first thing that must be considered is the stress-strain behavior of an individual lamina.

For an orthotropic lamina, the stresses and strains can be related through the reduced stiffness matrix, Q_{ij} with the coordinates, (x,y) corresponding to (1,2)

$$\begin{bmatrix}\sigma_1\\ \sigma_2\\ \tau_{12}\end{bmatrix} = \begin{bmatrix}Q_{11} & Q_{12} & 0\\ Q_{12} & Q_{22} & 0\\ 0 & 0 & Q_{66}\end{bmatrix} \cdot \begin{bmatrix}\epsilon_1\\ \epsilon_2\\ \gamma_{12}\end{bmatrix} \quad (1)$$

The Q_{16} and Q_{26} are zero because the normal only talks to normal and shear only talks to shear. The reduced stiffness Q_{ij} can be defined by the terms of the engineering constants

$$Q_{11} = \frac{E_1}{1-\nu_{12}\nu_{21}} \quad (2)$$

$$Q_{22} = \frac{E_2}{1-\nu_{12}\nu_{21}} \quad (3)$$

$$Q_{12} = \frac{E_2\nu_{12}}{1-\nu_{12}\nu_{21}} = \frac{E_1\nu_{21}}{1-\nu_{12}\nu_{21}} \quad (4)$$

$$Q_{66} = G_{12} \quad (5)$$

The transformed reduced stiffness $\bar{Q}_{ij}$ are related to the reduced stiffness by the transformation matrix as

$$\bar{Q}_{ij} = [T]^{-1}[Q][T]^{-\prime} \quad (6)$$

Where T is the transformation matrix and ‘ is the transpose of the matrix. The transformation matrix is defined as

$$T = \begin{bmatrix} \cos^2\theta & \sin^2\theta & 2\sin\theta\cos\theta \\ \sin^2\theta & \cos^2\theta & -2\sin\theta\cos\theta \\ -\sin\theta\cos\theta & \sin\theta\cos\theta & \cos^2\theta - \sin^2\theta \end{bmatrix} \tag{7}$$

After obtaining the transformed reduced stiffness, the stresses and strains can be related by,

$$\begin{bmatrix} \sigma_x \\ \sigma_y \\ \tau_{xy} \end{bmatrix} = \begin{bmatrix} \bar{Q}_{11} & \bar{Q}_{12} & \bar{Q}_{16} \\ \bar{Q}_{12} & \bar{Q}_{22} & \bar{Q}_{26} \\ \bar{Q}_{16} & \bar{Q}_{26} & \bar{Q}_{66} \end{bmatrix} \cdot \begin{bmatrix} \epsilon_x \\ \epsilon_y \\ \gamma_{xy} \end{bmatrix} \tag{8}$$

The stress-strain relations that the transformed reduced stiffness show in arbitrary in-plane coordinates are very useful in the definition of the laminate stiffness. This is because of the arbitrary orientation of the constituent laminae. Both the reduced stiffness and transformed reduced stiffness can be thought of as the k^{th} layer of a multilayered laminate.

$$\{\sigma\}_k = [\bar{Q}]_k \cdot \{\epsilon\}_k \tag{9}$$

It is important to note that the $\bar{Q}_{ij}$ can be different for each layer of the laminate, so the stress variation through the laminate thickness is not necessarily linear, even though the strain variation is linear.

Once the stress and strain relationships are identified through the reduced and transform reduced stiffness, the resultant laminate forces and moments are determined, where N is the force and M is the moments.

$$N = \begin{bmatrix} N_x \\ N_y \\ N_{xy} \end{bmatrix} \tag{10}$$

$$M = \begin{bmatrix} M_x \\ M_y \\ M_{xy} \end{bmatrix} \tag{11}$$

The resultant forces and moments are obtained by the integration of stresses in each layer or lamina through the laminate thickness, for example,

$$N_x = \int_{\frac{-t}{2}}^{\frac{t}{2}} \sigma_x dz \tag{12}$$

$$M_x = \int_{\frac{-t}{2}}^{\frac{t}{2}} \sigma_x z dz \tag{13}$$

More often times than not the stiffness matrix for a lamina is often constant within the lamina and in this case the forces and moments can be written as,

$$\begin{bmatrix} N_x \\ N_y \\ N_{xy} \end{bmatrix} = \sum_{k=1}^{N} \begin{bmatrix} \bar{Q}_{11} & \bar{Q}_{12} & \bar{Q}_{16} \\ \bar{Q}_{12} & \bar{Q}_{22} & \bar{Q}_{26} \\ \bar{Q}_{16} & \bar{Q}_{26} & \bar{Q}_{66} \end{bmatrix}_k \cdot \left[\int_{Z_{k-1}}^{Z_K} \begin{bmatrix} \epsilon_x^o \\ \epsilon_y^o \\ \epsilon_{xy}^o \end{bmatrix} dz + \int_{Z_{k-1}}^{Z_K} \begin{bmatrix} \kappa_x \\ \kappa_y \\ \kappa_{xy} \end{bmatrix} z \cdot dz \right] \tag{14}$$

$$\begin{bmatrix} M_x \\ M_y \\ M_{xy} \end{bmatrix} = \sum_{k=1}^{N} \begin{bmatrix} \bar{Q}_{11} & \bar{Q}_{12} & \bar{Q}_{16} \\ \bar{Q}_{12} & \bar{Q}_{22} & \bar{Q}_{26} \\ \bar{Q}_{16} & \bar{Q}_{26} & \bar{Q}_{66} \end{bmatrix}_k \cdot \left[\int_{Z_{k-1}}^{Z_K} \begin{bmatrix} \epsilon_x^o \\ \epsilon_y^o \\ \epsilon_{xy}^o \end{bmatrix} z \cdot dz + \int_{Z_{k-1}}^{Z_K} \begin{bmatrix} \kappa_x \\ \kappa_y \\ \kappa_{xy} \end{bmatrix} z^2 \cdot dz \right] \tag{15}$$

Theϵ_x^o, $\epsilon_y^o, \epsilon_{xy}^o, \kappa_x, \kappa_{y,}$and κ_{xy} are non functions of z, but are middle surface values. If the stiffness matrix for a lamina is not constant through the thickness of the lamina, for example a temperature or moisture gradient exists and the lamina material properties are temperature dependent, then $\left[\bar{Q}_{ij}\right]_k$ is a function of z and must be left inside the integral. However, if the stiffness of the matrix is constant, the ϵ_x^o, $\epsilon_y^o, \epsilon_{xy}^o, \kappa_x, \kappa_{y,}$and κ_{xy} values can be pulled out of the integral and the forces and moments can be defined as

$$\begin{bmatrix} N_x \\ N_y \\ N_{xy} \\ M_x \\ M_y \\ M_{xy} \end{bmatrix} = \begin{bmatrix} A_{11} & A_{12} & A_{16} & B_{11} & B_{12} & B_{16} \\ A_{12} & A_{22} & A_{26} & B_{12} & B_{22} & B_{26} \\ A_{16} & A_{26} & A_{66} & B_{16} & B_{26} & B_{66} \\ B_{11} & B_{12} & B_{16} & D_{11} & D_{12} & D_{16} \\ B_{12} & B_{22} & B_{26} & D_{12} & D_{22} & D_{26} \\ B_{16} & B_{26} & B_{66} & D_{16} & D_{26} & D_{66} \end{bmatrix} \cdot \begin{bmatrix} \epsilon_x^o \\ \epsilon_y^o \\ \epsilon_{xy}^o \\ \kappa_x \\ \kappa_y \\ \kappa_{xy} \end{bmatrix} \tag{16}$$

The A_{ij} matrix, which is the extensional stiffness, is defined as

$$A_{ij} = \begin{bmatrix} A_{11} & A_{12} & A_{16} \\ A_{12} & A_{22} & A_{26} \\ A_{16} & A_{26} & A_{66} \end{bmatrix} = \sum_{k=1}^{N} \begin{bmatrix} \bar{Q}_{11} & \bar{Q}_{12} & \bar{Q}_{16} \\ \bar{Q}_{12} & \bar{Q}_{22} & \bar{Q}_{26} \\ \bar{Q}_{16} & \bar{Q}_{26} & \bar{Q}_{66} \end{bmatrix}_k (z_k - z_{k-1}) \tag{17}$$

where $A_{16}$and A_{26} are shear-extension coupling

The B_{ij} matrix, which is the bending-extension coupling stiffness, is defined as

$$B_{ij} = \begin{bmatrix} B_{11} & B_{12} & B_{16} \\ B_{12} & B_{22} & B_{26} \\ B_{16} & B_{26} & B_{66} \end{bmatrix} = \frac{1}{2} \sum_{k=1}^{N} \begin{bmatrix} \bar{Q}_{11} & \bar{Q}_{12} & \bar{Q}_{16} \\ \bar{Q}_{12} & \bar{Q}_{22} & \bar{Q}_{26} \\ \bar{Q}_{16} & \bar{Q}_{26} & \bar{Q}_{66} \end{bmatrix}_k ({z_k}^2 - {z_{k-1}}^2) \tag{18}$$

where $B_{16}$and B_{26} is the bend-twist coupling.

The D_{ij} matrix, which is the moment coupling stiffness, is defined as

$$D_{ij} = \begin{bmatrix} D_{11} & D_{12} & D_{16} \\ D_{12} & D_{22} & D_{26} \\ D_{16} & D_{26} & D_{66} \end{bmatrix} = \frac{1}{3} \sum_{k=1}^{N} \begin{bmatrix} \bar{Q}_{11} & \bar{Q}_{12} & \bar{Q}_{16} \\ \bar{Q}_{12} & \bar{Q}_{22} & \bar{Q}_{26} \\ \bar{Q}_{16} & \bar{Q}_{26} & \bar{Q}_{66} \end{bmatrix}_k ({z_k}^3 - {z_{k-1}}^3) \tag{19}$$

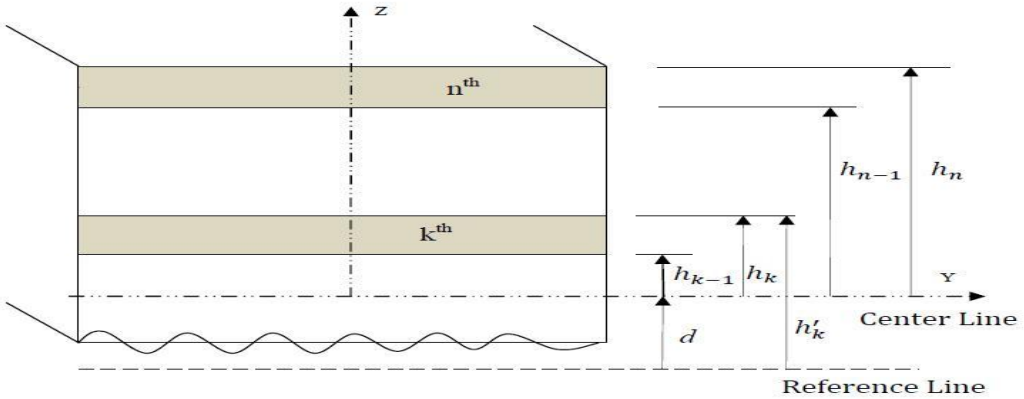

Figure 16: In order to determine the grand vector matrix, the coordinate notations of individual plies must be known.[10]

Once the general equations for stresses and strains on a composite laminate are determined, it is critical to transform this analysis toward the specific cross-sectional geometry of the member in question. For this project, a box beam geometry is selected to withstand the particular loads and bending moments. For this type of beam, the equivalent axial stiffness is of great importance. From the axial stiffness of the beam, the corresponding stresses and strains can be determined.

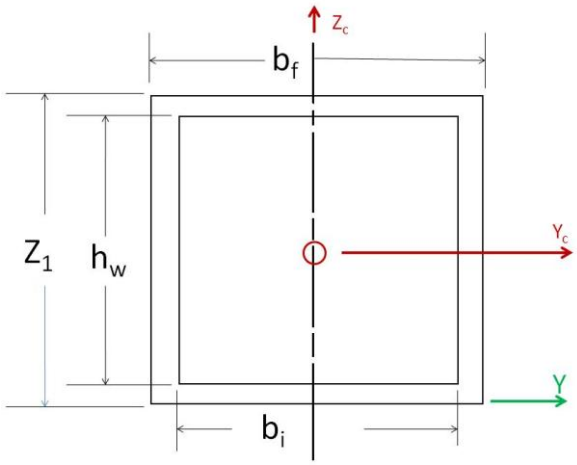

Figure 17: This figure shows the boxed beam diagram.[10]

Analysis begins by subdividing the geometry of the box beam into four sections: the top flange, bottom flange, left web, and right web. The axial force and bending moment equations for the top flange are given respectively by

$$N_{x1} = A^*_{1,f1}\mathring{\varepsilon}_{x,f1} + B^*_{1,f1}K_{x,f1} \tag{20}$$

$$M_{x1} = B^*_{1,f1}\mathring{\varepsilon}_{x,f1} + D^*_{1,f1}K_{x,f1} \tag{21}$$

Where $A^*_{1,f1}$, $B^*_{1,f1}$, $D^*_{1,f1}$are referred to as the axial, coupling, and bending stiffnesses of the beam and are defined as

$$A^*_{1,f1} = \frac{1}{a_{11}-\frac{b_{11}^2}{d_{11}}} \tag{22}$$

$$B^*_{1,f1} = \frac{1}{b_{11}-\frac{a_{11}d_{11}}{b_{11}}} \tag{23}$$

$$D^*_{1,f1} = \frac{1}{d_{11}-\frac{b_{11}^2}{a_{11}}} \tag{24}$$

Similarly, the axial forces and bending moments for the bottom flange are respectively defined as

$$N_{x2} = A^*_{1,f2}\mathring{\varepsilon}_{x,f1} + B^*_{1,f2}K_{x,f1} \tag{25}$$

$$M_{x2} = B^*_{1,f2}\mathring{\varepsilon}_{x,f2} + D^*_{1,f2}K_{x,f2} \tag{26}$$

However, the left and right webs of the box beam have

$$K_{x,lw} = 0 \tag{27}$$

$$K_{x,rw} = 0 \tag{28}$$

So as a result, the axial and bending moment equations for the web portions reduce to

$$N_{x,lw} = A^*_{1,lw}\mathring{\varepsilon}_{x,lw} \tag{29}$$

$$M_{x,lw} = B^*_{1,lw}\mathring{\varepsilon}_{x,lw} \tag{30}$$

$$N_{x,rw} = A^*_{1,rw}\mathring{\varepsilon}_{x,rw} \tag{31}$$

$$M_{x,rw} = B^*_{1,rw}\mathring{\varepsilon}_{x,rw} \tag{32}$$

The axial force applied through the centroid of the beam results in an expression for equivalent axial stiffness, $\overline{EA}$. The net total force in the x-direction is written as

$$\overline{N_x} = \overline{EA}\varepsilon^c_x \tag{33}$$

Where the equivalent axial stiffness of the entire cross-section is denoted as $\overline{EA}$ and ε^c_x is the strain at the centroid of the beam in the x-direction. Substituting each axial force into the generalized equation above results in

$$\overline{N_x} = b_{f1}\left(A^*_{1,f1}\mathring{\varepsilon}_{x,f1} + B^*_{1,f1}K_{x,f1}\right) + b_{f2}\left(A^*_{1,f2}\mathring{\varepsilon}_{x,f1} + B^*_{1,f2}K_{x,f1}\right) \tag{34}$$

It is important to note the strain for all the laminates are equal along the x-axis, so this suggests

$$\mathring{\varepsilon}_{x,f1} = \mathring{\varepsilon}_{x,f2} = \mathring{\varepsilon}_{x,lw} = \mathring{\varepsilon}_{x,rw} = \varepsilon^c_x \tag{35}$$

In addition, all the laminates assume no radius of curvature because of symmetry. Consequently,

$$K_{x,f1} = K_{x,f2} = K_{x,lw} = K_{x,rw} = 0 \tag{36}$$

Therefore the axial equation can be written as

$$\overline{N_x} = \left[b_{f1}\left(A^*_{1,f1}\right) + b_{f2}\left(A^*_{1,f2}\right) + h_w\left(A^*_{1,lw} + A^*_{1,rw}\right)\right]\varepsilon^c_x \tag{37}$$

By comparing the two axial force equations obtained, the equivalent axial stiffness can be calculated as

$$\overline{EA} = \left[b_{f1}\left(A^*_{1,f1}\right) + b_{f2}\left(A^*_{1,f2}\right) + h_w\left(A^*_{1,lw} + A^*_{1,rw}\right)\right] \tag{38}$$

The stresses and strains in the layers of the flange laminates can finally be calculated using the equivalent axial stiffness. Specifically, the stress and strain of any given layer in the flange laminates can be found by finding the mid-plane strain and curvature radius for laminates. Defining a load acting at the centroid of the beam, P, and considering the equivalent axial stiffness can assist in calculating the stresses and strains. In matrix form, this is expression is defined as

$$P = \overline{N_x} = \overline{EA}\varepsilon^c_x \quad \text{and} \quad \overline{M_x} = 0 \tag{39}$$

$$\begin{bmatrix}\overline{N_x} \\ \overline{M_x}\end{bmatrix} = \begin{bmatrix}\overline{EA} & 0 \\ 0 & D^c_x\end{bmatrix}\begin{bmatrix}\varepsilon^c_x \\ K^c_x\end{bmatrix} \tag{40}$$

Therefore,

$$\varepsilon_x^c = \frac{P}{\overline{EA}} \qquad \text{and} \qquad K_x^c = 0 \tag{41}$$

For the top and bottom flanges, the matrix form equation is defined as

$$\begin{bmatrix} \overset{\circ}{\varepsilon}_{x,fl} \\ \overset{\circ}{\varepsilon}_{y,fl} \\ \overset{\circ}{\gamma}_{xy,fl} \\ K_{x,fl} \\ K_{y,fl} \\ K_{xy,fl} \end{bmatrix} = \begin{bmatrix} a_{11} & b_{11} & b_{16} \\ a_{12} & b_{21} & b_{26} \\ a_{16} & b_{61} & b_{66} \\ b_{11} & d_{11} & a_{11} \\ b_{11} & d_{12} & d_{26} \\ b_{16} & d_{61} & d_{66} \end{bmatrix}_{sl} \begin{bmatrix} N_{x,fl} \\ M_{x,fl} \\ M_{x,fl} \end{bmatrix} \tag{42}$$

Where the *sl* subscript denotes the particular sub-laminate of the box beam and $M_{xy1}$is defined as

$$M_{xy,fl} = -\frac{1}{d_{66}} \left[b_{16} N_{x1} + d_{61} M_{x1} \right] \tag{43}$$

The strain in each flange can therefore be determined by using the equation

$$\left[\varepsilon_{fl}\right]_k = \left[\overset{\circ}{\varepsilon}\right]_{fl} + z_{k,fl} \begin{bmatrix} k_{x,fl} \\ k_{y,fl} \\ k_{xy,fl} \end{bmatrix}_{fl} \tag{44}$$

Where the subscript *fl* denotes either the top or bottom flange, $z_{k,fl}$ is the position of kth layer from the mid-plane of the sub-laminate. By expanding this

$$\begin{pmatrix} \varepsilon_{x,fl} \\ \varepsilon_{y,fl} \\ \varepsilon_{xy,fl} \end{pmatrix} = \begin{pmatrix} \overset{\circ}{\varepsilon}_{x,fl} \\ \overset{\circ}{\varepsilon}_{y,fl} \\ \overset{\circ}{\varepsilon}_{xy,fl} \end{pmatrix} + z_{k,fl} \cdot \begin{pmatrix} k_{x,fl} \\ k_{y,fl} \\ k_{xy,fl} \end{pmatrix}_{fl} \tag{45}$$

To determine the stress in the kth layer, lamination theory is used to identify the equation

$$\left[\sigma_{fl}\right]_k = \left[\bar{Q}\right]_{k,fl} \cdot \left[\varepsilon_{fl}\right]_k \tag{46}$$

The stresses in the web laminate using equivalent axial stiffness, $\overline{EA}$.

For the web laminate under axial loading

$$K_{x,w} = 0 \tag{47}$$

Therefore

$$\varepsilon_{x,w}^c = \varepsilon_x^c = \frac{P}{\overline{EA}} \tag{48}$$

So the force and moment equations in the laminate are mentioned earlier

$$N_{x,lw} = A_{1,lw}^* \overset{\circ}{\varepsilon}_{x,lw} \tag{49}$$

$$M_{x,lw} = B_{1,lw}^* \overset{\circ}{\varepsilon}_{x,lw} \tag{50}$$

$$N_{x,rw} = A^*_{1,rw}\varepsilon^{\circ}_{x,rw} \tag{51}$$

$$M_{x,rw} = B^*_{1,rw}\varepsilon^{\circ}_{x,rw} \tag{52}$$

If the web laminate is symmetrical, then $B^*_{1,lw/rw}$ is zero then it is important to note that

$$M_{x,lw/rw} = 0 \tag{53}$$

Once these forces and moments are obtained, the stress and strain in different layers of the web laminate can be calculated using the equations mentioned previously.

The three point and four point bend test was employed in this experiment. The experiment follows the test standards of the American Society for Testing and Materials (ASTM), under the test standards for the Standard Test Method for Flexural Properties of Unreinforced and Reinforced Plastics and Electrical Insulating Materials by Four-Point Bending, reference #D6272–10.[2] The test method utilizes tests for two different span loadings, the one-third support span and the one-quarter support span. Figure 18 shows the two distinctive support spans. The one-third support span was chosen in order to best fit the dimensions of the given four-point bending test instrumentation of the Instron machine. Specimens were tested for each scenario, well within the standard five specimens. The rate of crosshead motion *R* is shown in Eq. (54). The variable *L* refers to the support span, *d* refers to the depth of the beam, and *Z* refers to the rate of straining of the outer fibers. The rate of straining of the outer fibers Z is equal to 0.01.

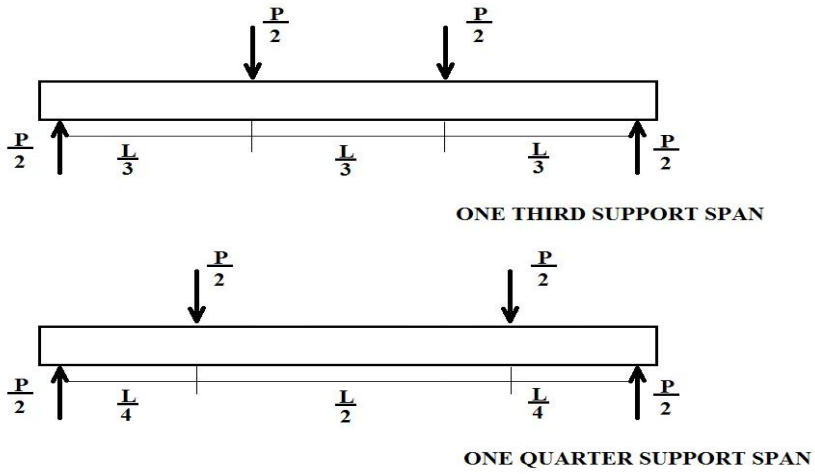

Figure 18: the two distinctive support spans: the one third support span and the one quarter support span.[17]ASTM PAPER

$$R = \frac{0.167ZL^2}{d} \tag{54}$$

When a beam is loaded in flexure at two central points and supported at two outer points, the maximum stress in the outer fibers occurs between the two central loading points that define the load span. The stress in the one third support span case is shown in Eq. (8). The variable *P* refers to the load at a given point on the load deflection curve, *L* refers to the support span, *b* refers to the width of the beam, and *d* refers to the depth of the beam. The flexural strength is equal to the maximum stress *S* at the moment of fracture

$$S = \frac{PL}{bd^2} \tag{55}$$

The maximum strain in the outer fibers also occurs at the mid-span. The maximum strain in the outer fibers *r* can be calculated in Eq. (9) for the one third support span case. The variables *Y* refer to maximum deflection of the center of the beam, *L* refers to the support span, and *d* refers to the depth.

$$r = \frac{4.70Yd}{L^2} \tag{56}$$

With the given variables, we are able to calculate the experimental data from the Instron machine.

Results and Discussion

Now that the structure of the hover board has been established we also needed to determine our propulsion system. During the early stages of design of the hover board we looked at many ideas that would provide the required lifting force. The first idea that we focused on in the first iteration of the design was using a single rotor stator compressor pair. We acquired this idea from a previous senior project that was conducted as a feasibility study for an electric powered jet pack.[1] This senior project proved, theoretically that it is possible to provide enough lift for an electric jet pack from a single rotor stator pair. We then developed a code that optimizes the power required for a given thrust using the axial compressor equations. After weeks of working on this code we realized that using the compressor stage was unfeasible because the power required from the electrical motors was enormous. We also had conversations with a Cal Poly graduate student that reinforce the fact that using the axial compressor stage would require too much power. Something else that deemed this design unfeasible is the added weight of an axial compressor. Another issue we ran into was finding locations where we can actually have these compressors manufactured as they would be too difficult to be manufactured here at Cal Poly. After running into all these issues with the single rotor stator pair, we decided to further investigate the available options for our propulsion system.

During the next iteration of the hover board we decided to stay traditional to regular hovercrafts. Current hover crafts use fan technology to provide the required lift but usually these power requirements are not so huge because of the use of the skirt. Since we already stated that our project would not require the use of a skirt, the power requirements for our hover board will be significantly larger than current hovercrafts. In order to determine if the implementation of the fan technology is feasible, we needed to design an optimized propeller that would provide the required thrust. In order to accomplish this, we used javaprop since the design and optimization of propellers is a very difficult task and we have not yet learned this. In javaprop we tried many configurations for our propellers. We varied the number of blades, the RPM, and the diameter of our inlet duct. We had the option to input the horsepower provided from our chosen motors. Something that is important to mention is that javaprop also has the option to vary the inlet velocity and then in optimizes the propeller to that velocity. We also noticed that the thrust produced by the propellers at the design velocity was nearly the same as the static thrust produced by the propellers because the design velocities were really low. The reason we couldn't choose a velocity of zero was that javaprop would not give us any answers using this velocity.

When it comes to our propulsion system we learned that the main driver is the electric motor. The motor is the main requirement because it is simple to get a high horsepower motor but with the expense of a lot of weight. The lighter electric motors do not provide the required power hover the board. After much research we decided that a five horsepower motor is the most power we can get without a huge increase in weight of the motor. Using five horsepower as our provided power, we designed our propellers in javaprop. The characteristics of the propellers are shown in

Table **1** and
Table 2.

Table 1: JavaProp Propeller Conditions for the 5 hp electric motor.

# of blades	Rotation Speed (RPM)	Diameter (m)	Velocity (m/s)	Power (W)
6	8,000	.28575	4.4	3728

Table 2: Optimized propeller characteristics for the 5 hp electric motor.

Airfoil	ARA D 6%, Re=50,000	**β at 75%R**	11.8°
Angle of attack	-3°	**v/(ΩR)**	.037
v/(nD)	.115	**Loading**	Very high
Efficiency	21.47%	**C_t**	1.2568
Static Thrust	181.89 N	**C_p**	.676
Power	3.73 kW	**Pitch**	141 mm

This specific propeller design provides 181.89 Newtons of thrust which translates to about 40.87 lbs for each propeller. The hover board will have 4 propeller assemblies therefore the total force provided for the hover board is 163.48 lbs. We realized that the five horsepower motor does not provide enough thrust to lift the weight of the board and a person. As mentioned previously, we are restricted by the electric motors. Since we are only able to produce 163 lbs of thrust using the five horsepower motor, we have decided not hover a person but, in order to have a proof of concept, we are still going to continue the construction of the hover board but being able to hover a set amount of weight. We decided to do this because we also realized that the technology of electric motors is greatly improving. In recent years, Oxford University has been in the process of developing a new lightweight and powerful electric motor. Their current concept is used in some automobiles and provides 67 hp and only weighs 28 lbs. Another great advantage of this motor is that it has an efficiency of 97%. This new electric motor technology is just the technology that the hover board demands. For future construction, the hover board would not be equipped with the heavy five horsepower electric motor but rather the new Yasa Oxford motor shown in fig. 19.. For future references, we determined the required horsepower to provide enough lift from the propellers.

Figure 19: A picture of the Oxford Yasa electric motor.[18]

In order to determine the required horsepower for the hover board we needed to conduct a ducted fan analysis. The ducted fan analysis is short and is an effective option. It will end up lighter, more efficient (due to the duct) and less chance of failure. We start the analysis already knowing what thrust we will need. It was decided that with the weight of the board, components, and rider, the thrust will need to be at least 400 lbs. Using adaptations of equations (57) and (58), we can find the velocity and then plug that into the mass flow rate equation:

$$\rho A V^2 = F \tag{57}$$

The mass flow rate is used into a power equation, assuming that the initial velocity is 0:

$$P = {}^1\!/_2\, \dot{m}\left(V_2{}^2 - V_1{}^2\right) \tag{58}$$

There are two possibilities regarding the sizing of the duct. The first is a constant area and the second is where the exit area is smaller, like a converging nozzle. The advantage of the smaller exit area is that it creates a larger velocity than a constant area duct; however the mass flow rate is lower. The power results of a constant area duct

can be seen in Fig. 20 while Figure . 21 shows how a smaller exit area affects the power. The goal is to get the lowest required power so that the batteries and motors we choose are as small as possible.

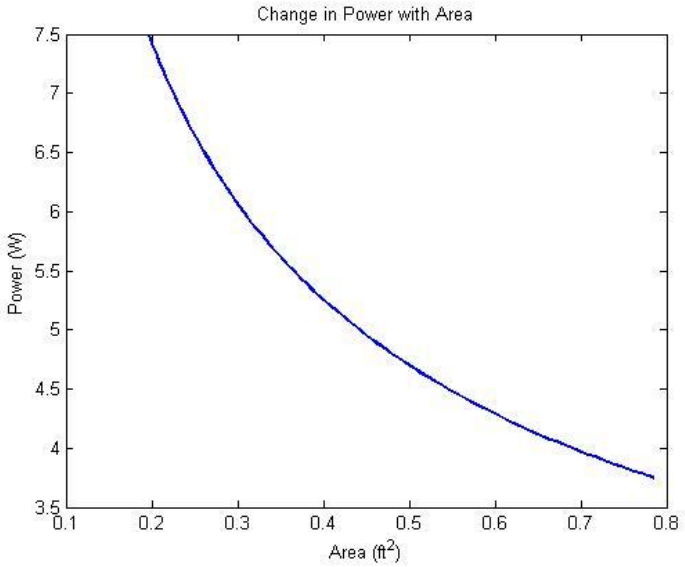

Figure 20: Power curve from a constant area ducted fan producing 400 lbs thrust

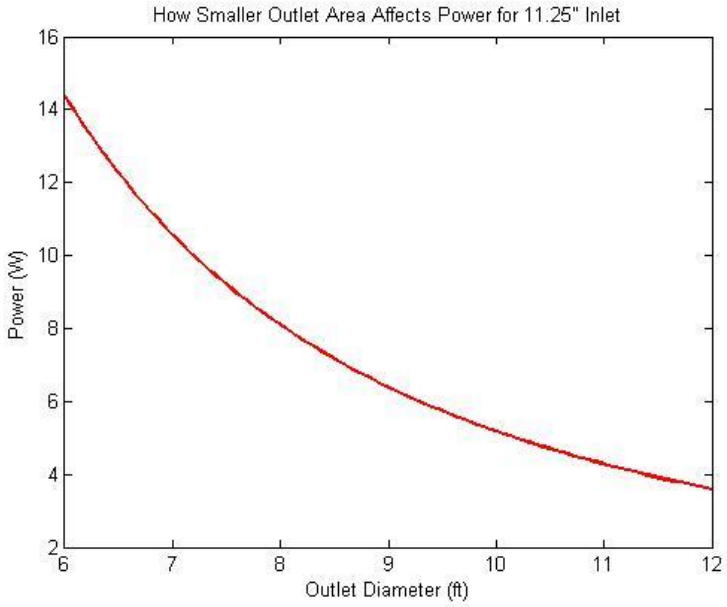

Figure 21: Power curve as outlet area decreases

Figure 21 shows that during the analysis, a smaller exit area increases the velocity but decreases the mass flow rate. Because power is dependent on mass flow rate and velocity, the velocity term is squared so it affects the power curve more. Thus, power required is much greater due to higher velocity when the exit area is smaller, which is not ideal. It was decided to choose a sizing configuration with a 5.75 inch constant radius. While the maximum inlet radius of 6 inches would be ideal, it would not fit on the model. This constant area configuration then yields a power requirement of 3.9 hp per fan assuming 100 percent efficiency but due to propeller efficiency this

requirement will increase greatly. From experience in JavaProp the propellers will end up with an efficiency of about 20 percent because of the small propeller radius. Approximating 20 percent efficiency, the hover board requires motors that output about 19.5 hp. This is easily accomplished using the Oxford electric motor. Since we will be using belts attached to the shafts of the propellers, one electric motor can be used for two propellers therefore instead of having 4 motors the hover board only requires 2 electric motors. We then went back to JavaProp and designed a brand new propeller to better accommodate the increase in horsepower. The properties of the propellers are summarized in Table 3 and Table 4.

Table 3: Propeller Conditions for the Oxford electric motor.

# of blades	Speed of rotation (RPM)	Diameter (m)	Velocity (m/s)	Power (W)
4	14,000	.28575	6	15,000

Table 4: Optimized propeller characteristics for Oxford electric motor.

Airfoil	Clark Y, Re=50,000	**β at 75%R**	19.1°
Angle of attack	1°	**v/(ΩR)**	.029
v/(nD)	.09	**Loading**	Very high
Efficiency	19.815%	**C_t**	1.1175
Static Thrust	495.28 N	**C_p**	0.5075
Power	15 kW	**Pitch**	234 mm

This propeller of design provides a maximum thrust of 495.28 Newtons which translates to 111.3 lbs for each fan. Since the hover board is equipped with four fan configurations the maximum thrust provided by the fans is 445.2 lbs. This is larger than is required to lift the hover board but it will be controlled by the throttle of the electric motors so we only use the required thrust not the maximum thrust.

We have shown that a propulsion system for the hover board is possible with future electric motor technology. The most impressive part of this is that the motors are extremely lightweight. Since we do not have the required funds to purchase the Oxford Yasa Motors we have decided to use the five horsepower motors that are available to us because we have the funds to purchase them. For proof of concept, we will be constructing the hover board with the five horsepower motors and applying a certain amount of weight to the hover board we will test the behavior of the hover board and the control issues associated with the hover board.

Now that we have the required power for the hover board we need to size the batteries that will be the power source for the electric motors. A trade study was conducted to choose the types of batteries to power the motors. The main requirement was that it would need to be rechargeable because they will eventually be located in a minimum access area within the board, and it would not be efficient to have to continuously change out the batteries after every use. The parameters used are based on the requirements of the hover board, ranking from highest weight to lowest:

1. Power (0.3/1)
2. Energy Density (0.25/1)
3. Charge/Discharge Efficiency (0.2/1)
4. Weight (0.2/1)
5. Life (0.05/1)

The goal is to choose a type of battery that will yield the most power and still be lightweight, which is why the first two parameters have the highest weight. A highly efficient battery would mean that when it charges and discharges the amount of power available stays roughly the same. The average weight, based on common applications will be important because the board requires the lightest combined weight possible. The life of the battery is weighted lowest because changing them out would be a lot of work; essentially, choosing a battery that

has a lifespan of a few years would be good so that if the batteries need to be replaced the process wouldn't happen very often shows Table 5 the trade study results using today's most common rechargeable battery options. Each score is out of 10 possible points.

Table 5: Trade Study for Rechargeable Batteries

	Lead Acid	**Alkaline**	**Ni-Cadmium**	**NiH_2/NiMH**	**Lithium-Ion**	**Li-Polymer**
Power (.3)	7(.3) = 2.1	5(.3) = 1.5	6(.3) = 1.8	8(.3) = 2.4	10(.3) = 3	10(.3) = 3
En. Den. (.25)	5(.25) = 1.25	7(.25) = 1.75	6(.25) = 1.5	7(.25) = 1.75	9(.25) = 2.25	8.5(.25) = 2.1
Eff. (.2)	6(.2) = 1.2	10(.2) = 2	6(.2) = 1.2	5(.2) = 1	8(.2) = 1.6	10(.2) = 2
Weight (.2)	4(.2) = .8	2(.2) = .4	4(.2) = .8	6(.2) = 1.2	9.5(.2) = 1.9	10(.2) = 2
Life (.05)	6(.05) = .3	5(.05) = .25	7(.05) = .35	10(.05) = .5	4(.05) = .2	4(.05) = .2
Total	**5.65**	**5.9**	**5.65**	**6.85**	**8.95**	**9.3**

The choice came down to two options, either Lithium-Ion batteries or Lithium-Polymer batteries. Lithium-Ion batteries came up short in the trade study but for our application would be more than enough, especially due to their high power-to-weight performance. While Lithium-Polymer batteries are more efficient, the technology has not yet been fully researched as far as larger applications. Manufacturing one for this application, which would need to be about 2 lbs for each motor based on the power-to-weight ratio, would be very expensive. In the end, Lithium-Ion batteries would be a much cheaper alternative at the moment and would only suffer slightly performance-wise. An example of a lithium-ion battery that will be utilized for the hover board can be seen in Fig. 22.

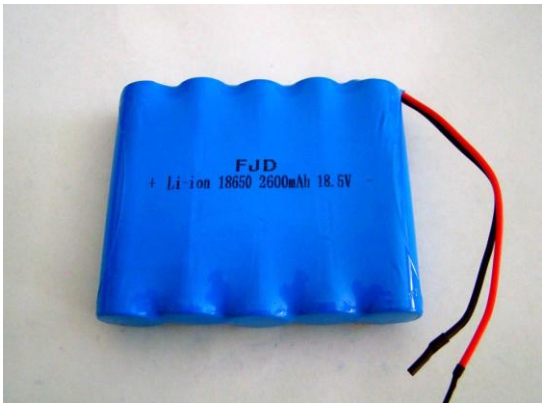

Figure 22: An example of a lithium-ion battery[19]

To figure out the size of the batteries, this equation is used:

$$W_{batt} = \frac{(Power\ req'd)(flight\ time)}{Specific\ energy} \tag{59}$$

The estimated flight time for the hover board is one minute. The specific energy for Li-Ion batteries was 250 Wh/kg. Plugging these values into equation (59) with power required in watts, flight time in hours, and specific energy in Wh/kg, yields a total weight of 3.42 lbs. This is an overestimation using 2 minutes, as the total running time will include turning on the engine, letting the engine reach maximum power, and allowing for troubleshooting while in the air. This is still well within the weight allowance for batteries.

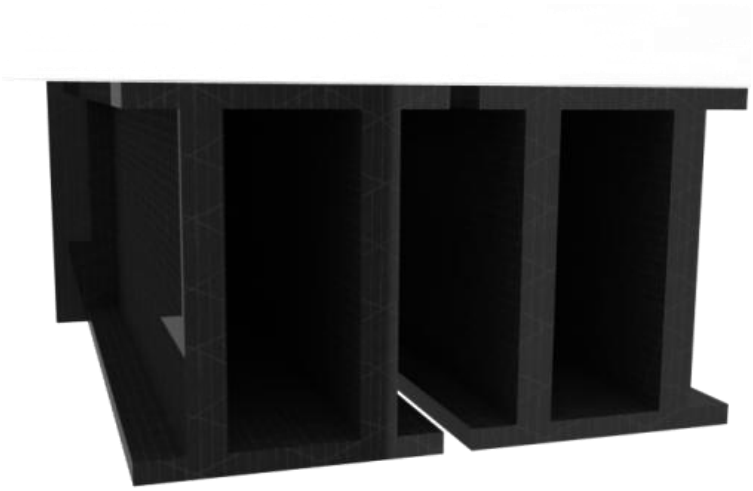

Figure 23: A cut view of the internal structure.

The next step in the design process was to design the structure of the hover board. In the first iteration of the hover board design we implemented a series of I-beams as the interior of the structure. For the current iteration of the design we decided that we needed to increase the torsional stiffness of the structure so we decided to incorporate box beams into the internal of the structure. We only used two internal box beams that ran the length of the hover board. A representation of the internal structure of the hover board is shown in Fig. 23.The figure shows the two boxed beams that comprise the internal structure of the hover board. There are two box beams with a maximum width of 10 inches and a height of 12 inches. The internal structure has a total width of 24 inches and a total length of 24 in. These dimensions do not include the size of the nacelles or the attachment plates. The thickness of the box beams is 0.5 in because the materials that are available to us have a thickness of 0.5 inches. The box beams are also constructed of a 2 ply-core-2 ply construction. The plies are made up of unidirectional carbon fiber and the core will be Nomex honeycomb.

We conducted a Finite Element Analysis on this box beam internal structure in which we assumed that the box beams are attached to the attachment plates and we treated that boundary as a fixed wall condition, which means that both ends of the internal structure are fixed to the wall. The program that was used to conduct the FEA analysis is Patran. The material that we are using for the hover board structure was donated by C&D Zodiac. They have many flat panel carbon fiber sandwiches. The drive to choosing this material was that it is already pre-constructed and the material properties are already known because C&D Zodiac had already conducted all of the material property testing. Knowing the material properties was helpful because we simply inputted them into the finite element model. We also simplified the analysis by utilizing the properties of symmetry. Since we assumed that the person would be loading both box beams the same then we only modeled one box beam and divided the load of the person by two which we then enforced on the beam. In conducting the analysis, we also assumed two different configurations. First we looked at the most common configuration in which the person standing on the board with the base of their feet spread open therefore the weight of the person is distributed onto the board through the surface area of the person's shoe. In this first case there are 42.5 lb forces acting on two separate areas of the box beam at 10% locations from the ends of the box beams. The finite element analysis of this configurations shows that the maximum displacement was 8.16×10^{-5} in. This maximum deflection occurs in the middle of each of the distributed loads. This small deflection is something that is also desired because composite materials are usually more brittle than metals therefore they break at smaller deflections. The finite element analysis results are shown in fig. 24. You can see the behavior of the structure when loaded and it also shows the stress distributions of the structure. If the hover board were to ever fail we would expect it to fail at the regions highlighted in colors closest to red because this is also where the largest deflection and the largest stresses are acting. The maximum stress acting on the structure was determined to be 90.6 psi. This stress distribution is shown in Fig. 25.

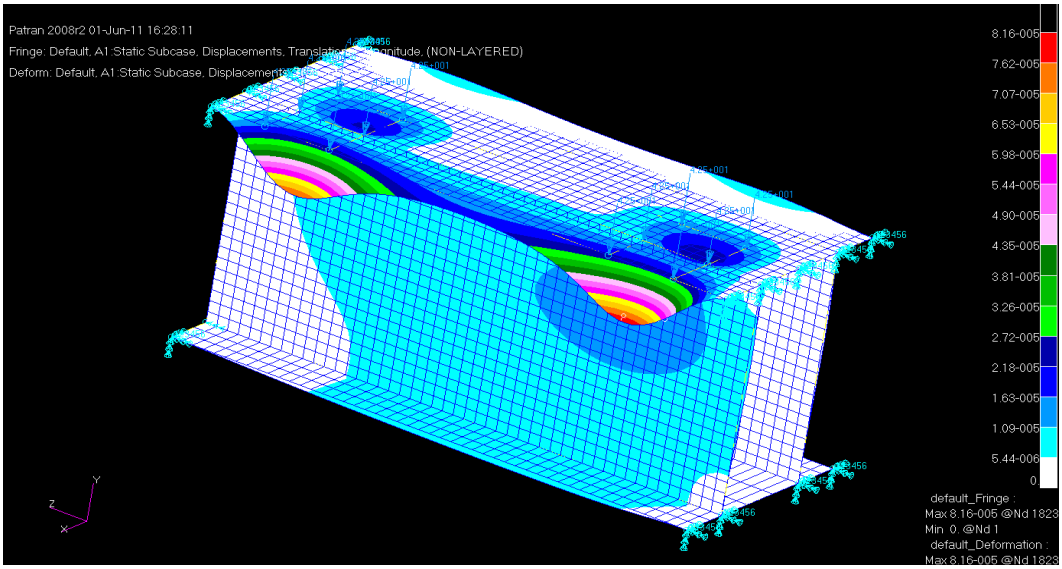

Figure 24: The displacement on the box beam is analyzed by Patran.

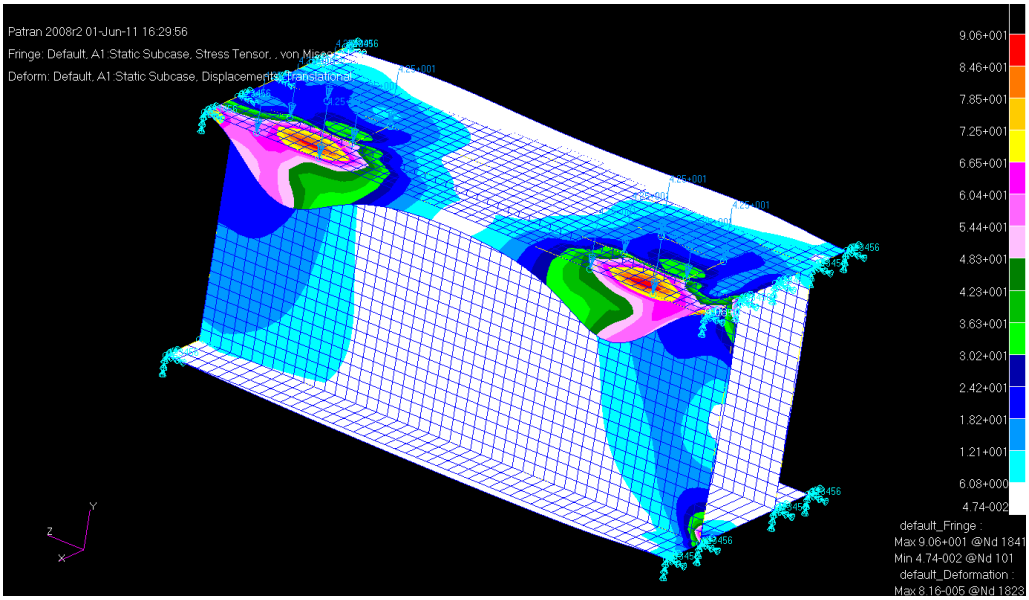

Figure 25: The stress on the box beam is analyzed by Patran.

The next case that we looked at was a worst case scenario in which the entire load is concentrated in the middle of the beam. This would mean that a force of 85 lb was applied to the middle of the box beam and then the analysis was conducted. After conducting the analysis the finite elements analysis shows that in the worst case scenario has a maximum deflection of 2.75 x 10^{-3}in. The maximum stress on the hover board was 3100 psi at the location of the flange of the box beam. This large psi is due to the fact that the load that was implemented in Patran was a line load but in reality the load would be distributed as the shoe of the person would not create a line load on

the structure. The worst case scenario makes us confident that the structure of the hover board will be able to withstand the loads imposed on the hover board. The deflection analysis is shown in fig. 26 and fig. 27.

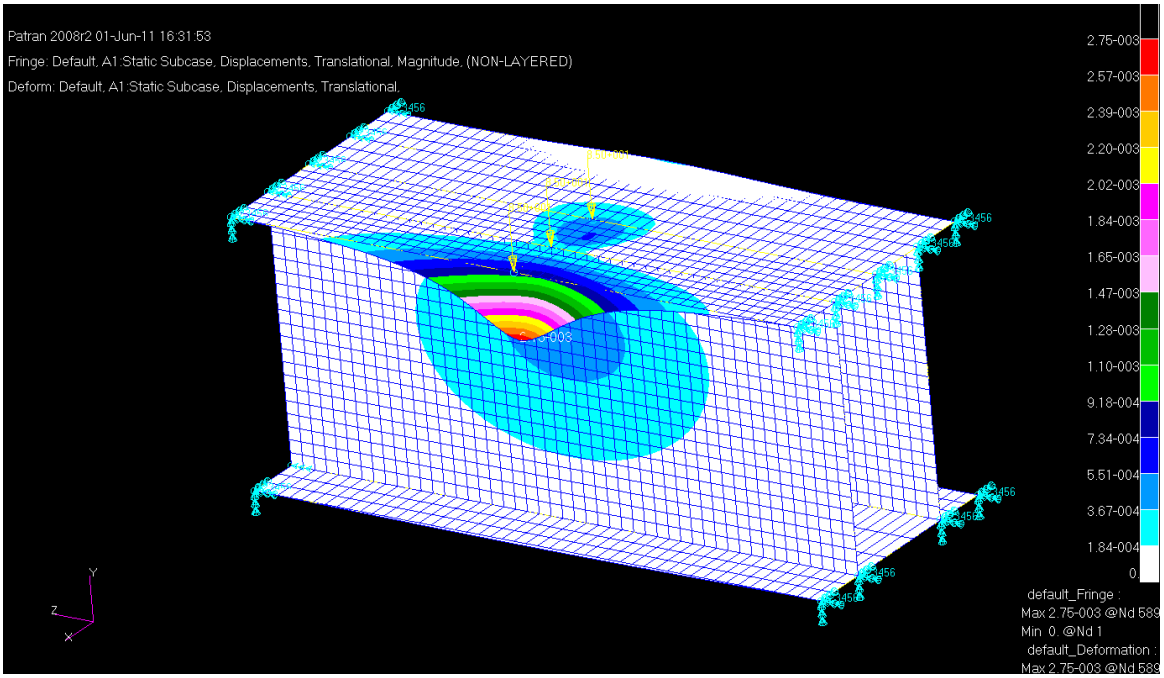

Figure 26: The displacement on the box beam at the worst case is analyzed by Patran.

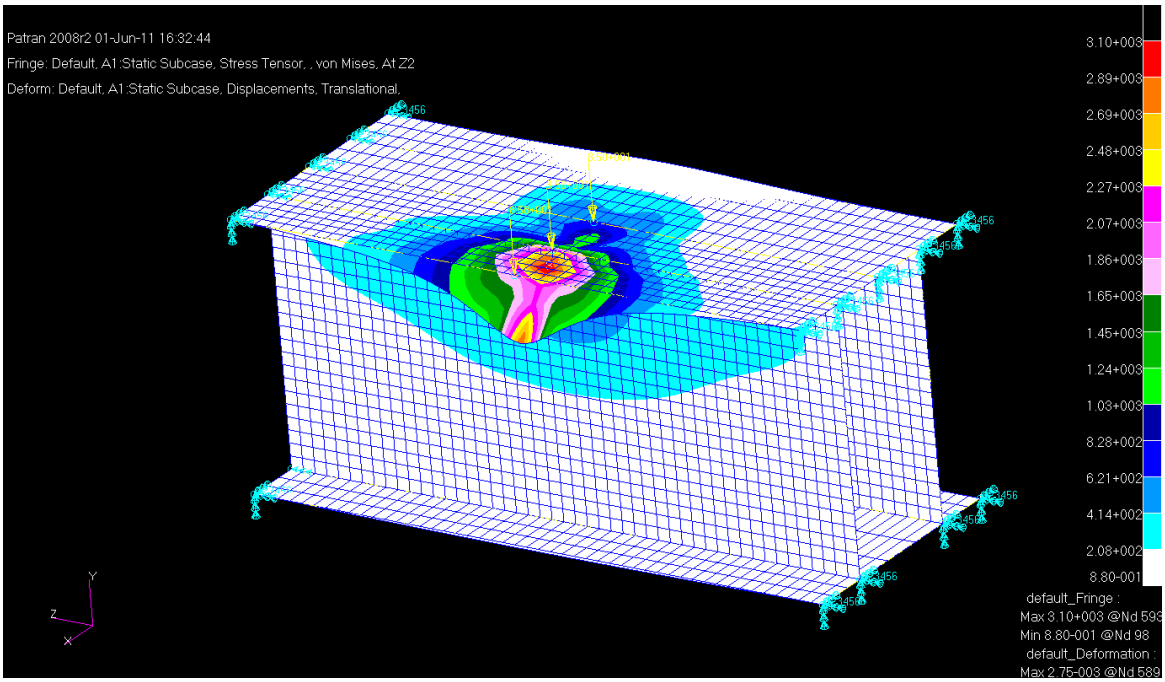

Figure 27: The stress on the box beam at the worst case is analyzed by Patran.

In order to determine the stresses and strains of the box beams in the hover board, it is essential to know certain material properties. A particular property of interest is the Young's Modulus based on the box beam's material and geometry. The Young's Modulus is necessary to complete the Q matrix for each lamina; consequently,

the Q matrix is used to calculate the A, B, and D matrices for every lamina. At that point, the forces and moments for each laminate are used to calculate the corresponding stresses and strains in the laminate.

To calculate the Young's Modulus for a box beam implemented in the hover board, test laminates of various material were fabricated and endured point loads in an Instron machine to obtain the appropriate stress-strain curve of the material. Test strips were fabricated to simulate the effects of a 160lb person standing on the hover board. After determining the stress-strain curves for each material and load configuration, the Young's Modulus can be calculated. The materials investigated include carbon fiber and fiber glass. Each test strip is composed of a core and a set number of fiber layers; the core and layers are joined through an epoxy adhesive mixture. Each test strip varied in size for every test, but the average size of each strip measured 0.6in thick, 0.8in wide, and 9.5in long. Loading configurations also varied for each material, so a 3-point bend and 4-point bend test were investigated. The 3-point bending test served to show the effects on the beams when applying a general point load at the center of the beam. More importantly, the 4-point bending test served to simulate the actual point loads experienced on the box beams by the weight of a person distributed over his/her 2 feet. It is important to note the Instron machine performed the test based on the test strip having roller supports at both of its ends. Although the actual hover board assembly will have the beams fixed at each end to a plate that is connected to the engine nacelles, the results of the test suggest this detail to be negligible in designing the beam.

The first material and load configuration is set as a fiber glass laminate under a 3-point bend test. Figure 28 illustrates the stress-strain curve for this particular experiment. It is important to note that the fiber glass strips for this experiment consisted of a 4-layer laminate. The red and maroon curves depict the experimental results of the strip being placed horizontal—that is with the thickness dimension pointing in the vertical direction. The purpose of this load placement is to simulate the effects that may occur on the flanges of the beam. Specimen 1, shown in red, had a thickness of 0.564in and a width of 0.865in. Specimen 2, illustrated in maroon, had a thickness of 0.564in and width of 0.823in. The maximum load endured by specimen 1 is shown to be about 110lb with a maximum deflection of about 0.275in; these results describe the better-performing strip between the two specimens. As expected, the main cause of failure was due to de-lamination of the fibers on the upper face of the strip under compression. From the specified curve, the value of Young's Modulus for this specimen under a 3-point bed test is 3,950psi. It is

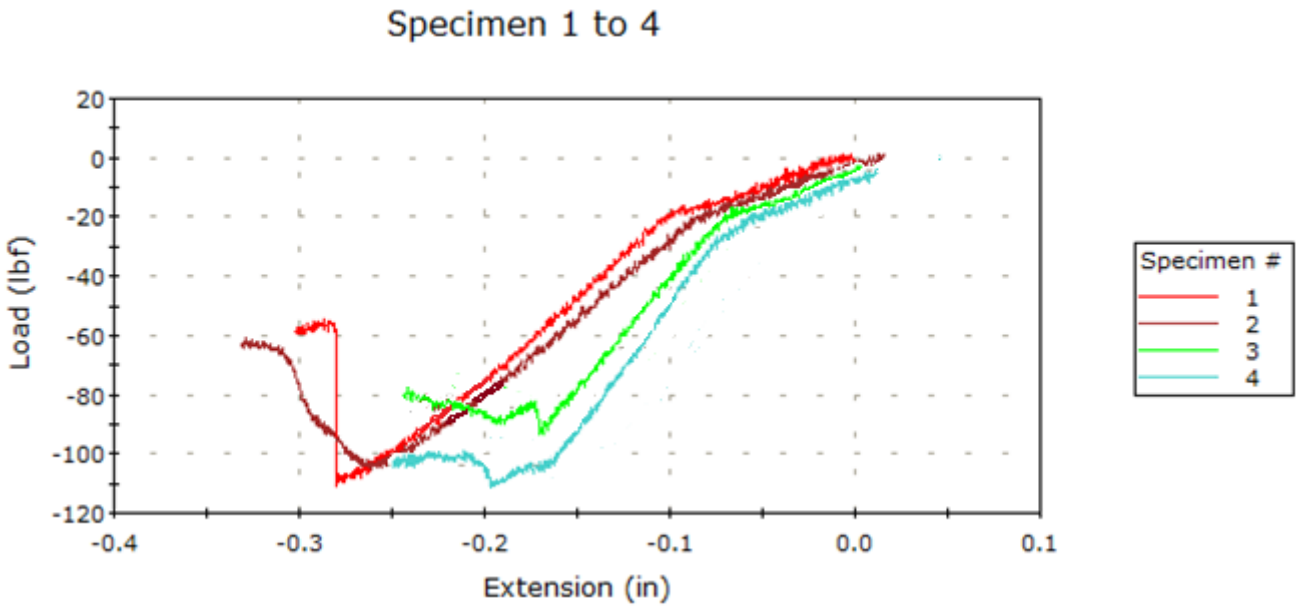

Figure 28: The stress-strain curve of a fiber glass laminate under 3-point bending to simulate flange and web loading.

understood that this *E* value is grossly small for what the expected Young's Modulus value should be for a laminate of this configuration. A possible explanation for such a low value is that the prepreg resin used to bond each layer

was of very low quality, so a strong bond between the layers could not be achieved. Second, the fiber material used for the test trip was expired—drastically depreciating the quality of the laminate and substantially decreasing performance.

The second configuration of the fiber glass laminate was put under a 3-point bend test. Figure 28 also illustrates the stress-strain curve for this particular experiment. Once again, the fiber glass strips for this experiment consisted of a 4-layer laminate. The placement of the strip was set in the Instron machine with the thickness value lying in the vertical position. Unlike the previous configuration, this load placement is to simulate the effects that may occur on the webs of the box beam. Specimens 3 and 4 are shown in the figure to share the same loading configuration. Specimen 3, shown in green, had a thickness of 0.821in and a width of 0.563in. Specimen 4, illustrated in blue, had a thickness of 0.863in and width of 0.566in. The maximum load endured by specimen 4 is shown to be about 105lb with a maximum deflection of about 0.165in; these results describe the better-performing strip between the two specimens. Again, the main cause of failure was due to de-lamination of the fibers on the upper face of the strip under compression. From the specified curve, the value of Young's Modulus for this specimen under a 3-point bed test is 6,178psi. It is understood that this *E* value is also very small for what the expected Young's Modulus value should be for a laminate of this configuration. A possible explanation for such a low value is that the prepreg resin used to bond each layer was of very low quality, so a strong bond between the layers could not be achieved. Second, the fiber material used for the test trip was expired—drastically depreciating the quality of the laminate and substantially decreasing performance.

The third material and load configuration was a carbon fiber laminate under a 3-point bend test. Figure 29 illustrates the stress-strain curve for this particular experiment. The carbon fiber laminate under this loading configuration was also composed of 4 layers. The curve depicts the experimental results of the strip being placed horizontal—that is with the thickness dimension pointing in the vertical direction. The purpose of this load placement is to simulate the effects that may occur on the flanges of the beam. The specimen had a thickness of 0.624in and a width of 0.824in. The maximum load endured by the specimen is shown to be about 140lb with a maximum deflection of about 0.325in. As expected, the main cause of failure was due to de-lamination of the fibers on the upper face of the strip under compression. This ultimately implied that failure due to de-lamination is a common theme for the box beam test strip—regardless of what material the beam is composed of.

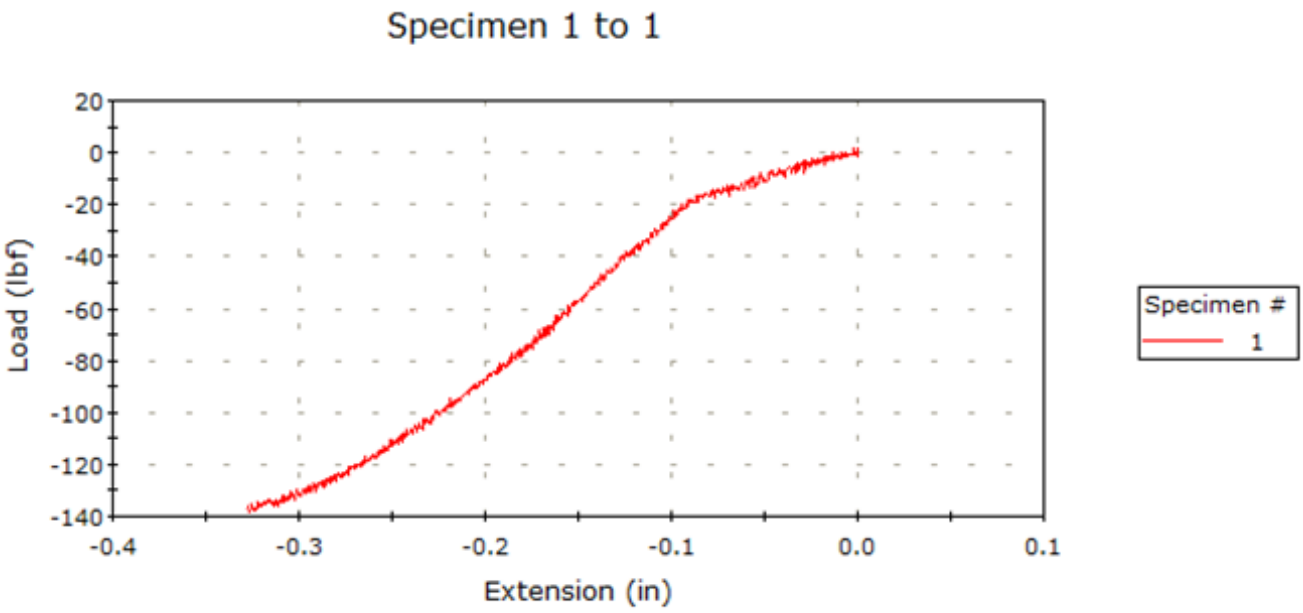

From the specified curve, the value of Young's Modulus for this specimen under a 3-point bed test is 509,609psi. Again, this *E* value is very small for what the expected Young's Modulus value should be for a laminate of this

configuration. Possible explanations for such a low value is that the prepreg resin used to bond each layer was of very low quality and the fiber material used for the test trips was expired—resulting in a laminate that had a significant decrease in performance.

The final material and load configuration was a carbon fiber laminate under a 4-point bend test. This experimental set-up is recognized to be the most accurate in simulating the bending effects the box beam will endure during real operational conditions. Figure 30 illustrates the stress-strain curve for this particular experiment. Once again, it is important to note that each carbon fiber specimen for this particular experiment consisted of a 4-layer laminate. The curves depict the experimental results of the strip being placed horizontal—that is with the thickness dimension pointing in the vertical direction. The purpose of this load placement is to simulate the effects that may occur on the flanges of the beam. The optimum performing specimen is selected to establish data for the best case scenario, so specimen 3 is selected to calculate the material's properties. Specimen 3, shown in green, had thickness and width lengths of comparable dimensions to the third configuration. The maximum load endured by specimen 3 is shown to be about 225lb with a maximum deflection of about 0.35in. As expected, the main cause of failure was due to de-lamination of the fibers on the upper face of the strip under compression. From the specified curve, the value of Young's Modulus for this specimen under a 4-point bend test is 899,715psi. It is understood that this *E* value is—once again—assumed to be undersized for what the expected Young's Modulus value should be for a laminate of this configuration. Causes for such a low *E* value is attributed to the same reasons mentioned previously. In other words, the prepreg resin used to bond each layer was of very low quality, so a strong bond between the layers could not be achieved. Lastly, the fiber material used for the test trip was expired—drastically depreciating the quality of the laminate and substantially decreasing performance.

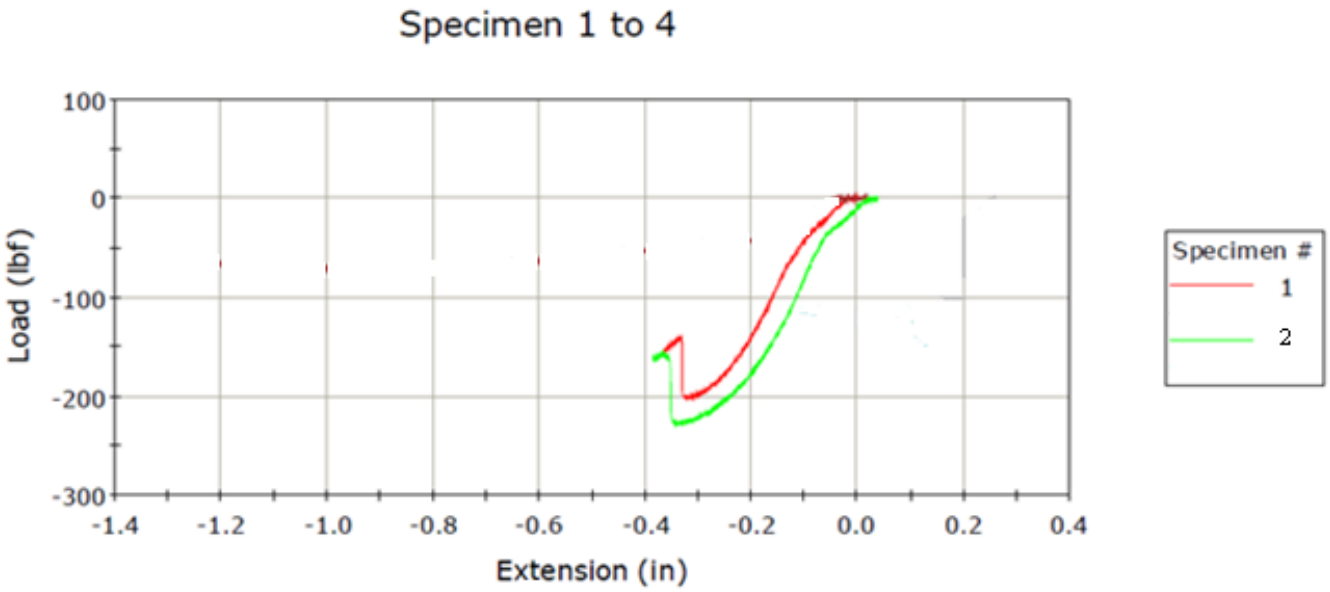

Figure 30: The stress-strain curve of a carbon fiber laminate under 3-point bending.

It is interesting to note the *E* values for all the experiments yielded expected values in relation to one another. The Young's Modulus for the fiber glass under 3-point bending is less than that of the carbon fiber under the same loading configuration. This result is expected because carbon fiber is known to be one of the best composite materials in terms of performance. Also, the high value of *E* for the fiber glass material in the second configuration under a 3-point bending test is calculated to be the highest among all the experiments. The reason for this result is that the specimen is capable of deflecting less for the same amount of force under that particular loading placement where the thickness of the test specimen is higher than the width. It is also important to note the

Young's Modulus for the carbon fiber under a 4-point bending test is higher than that of a 3-point bending test simply because the force is split at 2 points along the beam's length.

Now that the integrity of the internal structure of the hover board was proven to be plausible, we modeled a depiction of the entire hover board without including the outer skin of the board. We did not include the outer skin because it will be arbitrary. The skin is not designed to carry any of the loads therefore it is not a crucial part of the design and does not need to be accounted for. The parts of the hover board that were modeled were the internal structure, the nacelles in which the propellers are attached to. The model of the hover board is shown in fig. 31. The different major components of the hover board are color coded in significantly different colors in order to emphasize the difference between them. The internal dimensions of the hover board are as follows. The length of the hover board is 48 inches, the width is 24 inches, and the height of the hover board is 12 inches.

Figure 31: This picture shows an overall view of the hover board structure.

Bamboo Material

In order for the hover board to operate as predicted it is assumed that it will be comprised of a lightweight and strong material. This was accomplished through the use of a composite sandwich body with resulted in a strong, lightweight and stiff body. Aside from carbon composite sandwiches, a natural material like bamboo was studied further in order to determine if it would be a viable or an even better option for the internal structure of the hover board. The main issue with a natural material like bamboo is that it is difficult to find bamboo pieces with the exact same measurements like you would a piece of wood because bamboo grows in tubular form. Even along the same piece of bamboo, the inner and outer diameters are not the same. Similar to wood, there are different types of bamboo in the world, some are stronger than others. This indicates that each type of bamboo has its own mechanical properties that to this day are not all known. If a natural material like bamboo is to be considered as a viable

replacement for composite sandwiches, then it is important that the mechanical characteristics of the chosen bamboo be determined.

After careful searching, a few rods of bamboo were selected for testing. In order to legitimize the findings of the testing standard ASTM D4761-11 was followed. Although this standard was used for determining the mechanical characteristics of wood under compression, the standard was deemed applicable because there is no current standard to determine the mechanical characteristics of bamboo. The test pieces were cut to follow the standard, which states that the length of the test specimen must be fifteen times larger than the diameter of the bamboo rod. Also when conducting the test, the standard states that the bamboo must fail in no shorter than ten second and no longer than ten minutes. A rate of displacement was chosen to meet that requirement. The measurements in table 6 show that the bamboo is testable and that the measurements for each specimen are close to each other.

Table 6: Table of Measurements for each Specimen

Specimen	Length (in)	Max Diameter (in)	Min Diameter (in)	Avg Diameter (in)	Max Thickness (in)	Min Thickness (in)	Avg Thickness (in)	Joint
1	15.827	1.381	1.358	1.358	0.173	0.161	0.167	Yes
2	14.961	1.258	1.225	1.225	0.172	0.133	0.1525	Yes
3	16.142	1.494	1.464	1.464	0.2	0.185	0.1925	Yes
4	14.134	1.489	1.489	1.489	0.21	0.187	0.1985	Yes
5	10.315	1.597	1.421	1.421	0.278	0.234	0.256	Yes
6	11.811	N/A	N/A	1.358	0.213	0.2	0.2065	No
7	13.583	N/A	N/A	1.225	0.173	0.168	0.1705	No
8	12.992	N/A	N/A	1.464	0.161	0.141	0.151	No
9	9.252	N/A	N/A	1.489	0.149	0.143	0.146	No
10	8.465	N/A	N/A	1.421	0.232	0.204	0.218	No

The main characteristic that was sought after was Young's Modulus of the bamboo. In order to determine this value from the data acquired from the testing, it must be known that the modulus is the slope of the linear portion of the stress strain curve. This relationship is easily expressed in the equation below as

$$Young's Modulus = Slope\ of\ Stress - Strain\ Curve$$

or in mathematical terms

$$G = \frac{\Delta Stress}{\Delta Strain}$$

where G is Young's Modulus. The change in stress and strain can be determined by picking two separate points on the linear portion of the data and subtracting the stress values and the strain values. This method is shown below to be

$$G = \frac{Stress_2 - Stress_1}{Strain_2 - Strain_1}$$

where $Strain_2$ and $Stress_2$ are the values for the second point chosen and $Strain_1$ and $Stress_1$ are the values for the first point chosen.

A stress-strain curve is normally formulated from data acquired from a one dimensional tension test. In the case of the bamboo, it was easier to test under compression rather than tension. The difficulty of conducting a one dimensional tension test on a bamboo rod is the attachment method. There is no clear method that would allow for a tension test because of the cylindrical shape of the bamboo. By assuming that the bamboo is isotropic, then the data retrieved from a one dimensional compression test will yield results similar to a one dimensional tension test. The only difference between the tests is the direction of the force and deflection.

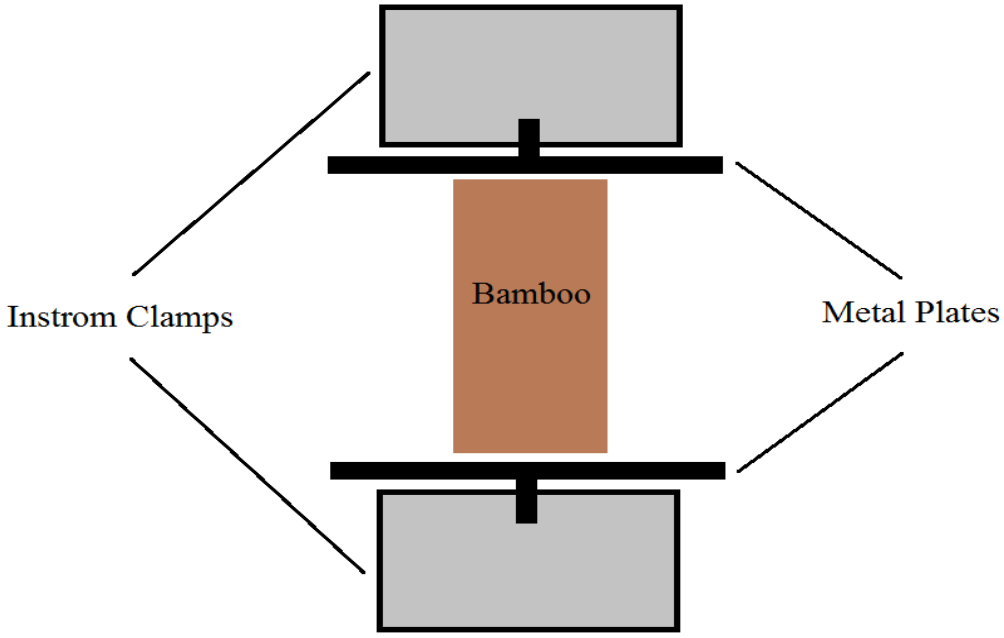

Figure 32: This is the set up of the 1-D axial compression test.

This experiment was conducted using an Instron machine. In order to allow for an even distribution of force onto the cross-section of the bamboo, metal plates were placed between the bamboo and the Instron clamps. The set-up for the test is shown in figure32.

Before conducting the test, a long piece of bamboo was chosen with a relatively similar circumference from top to bottom. The long rod was then cut into shorter pieces. Two types of short rods were cut. The first rods that were cut included the joint that bamboo is known to have. The other type of rod did not have joints. This was done in order to determine the effect the joint has on the mechanical properties of the bamboo. After cutting the bamboo, measurements were taken and recorded. The software for the Instron machine was the opened and a compression test was chosen. Before commencing with the test, metal plates were attached to the Instron machine's clamps as seen in figure 32. The bamboo specimens with joint were the first to be tested and then the specimens with no joints. The measurements were inputted into the Instron program before each test. The specimens were tested one at a time. After all the testing was finished the Instron machine was shut-off in the proper manner and the data collected was retrieved from the computer.

Utilizing the method described earlier, Young's Modulus was determined using the linear portion of the data. The modulus was computed for each of the specimens and then the average between all of the similar specimens was taken. The average Young's Modulus for the bamboo specimens with joints was 2309.5 ksi. The Max Load and the strain and stress at the max load were determined to be 7402.9 lb, .5732 % elongation, and 9.783

ksi, respectively. The standard deviation for each of these values is within reason except for the standard deviation for the maximum load. This may be to the fact that each of the specimens had different thicknesses and diameters. Also another factor that led to this was the accuracy of the cut. If the ends of the bamboo were not very close to 90 degrees then the load from the Instron machine would not have been transferred from the plates to the bamboo equally, therefore causing early yielding. The values for the specimens with joints are found in table 7.

Table 7: Test Results for Long Bamboo Specimens with Joints Under Compression

Specimen Label	Young's Modulus (ksi)	Max Load (lbf)	Strain @ Max Load (%)	Stress @ Max Load (ksi)
1	2620.81814	6895.36521	0.51166	10.92964
2	2288.69452	4248.99052	0.51348	8.14401
3	2000.43816	7721.75799	0.67080	9.92489
4	2471.42148	7291.46975	0.50161	9.14239
5	2166.28050	10857.19614	0.66843	10.77400
Average	2309.5306	7402.956	0.573196	9.782986
Standard Deviation	218.90704	2109.549	0.078833	1.040545

The values for the specimens without joints are located in table 8. The averages for these specimens were also determined and the values were similar to the specimens with joints. The Young's Modulus for these specimens was 2171.3 ksi. The maximum compressive load was 7394.1 lb and the corresponding strain and stress at that load were 0.726 % elongation and 10.17 ksi, respectively.

Table 8: Test Results for Long Bamboo Specimens without Joints under Compression

Specimen Label	Young's Modulus (ksi)	Max Compressive Load (lbf)	Compressive Strain @ Max Compressive Load (%)	Compressive Stress @ Max Compressive Load (ksi)
1	2538.07621	11247.17816	0.90368	13.43877
2	2248.78983	5780.84731	0.57045	8.16059
3	2440.30815	4864.99288	0.45782	8.22411
4	1868.28235	5595.19510	0.75444	10.09435
5	1761.09777	9482.15236	0.94528	10.93621
Average	2171.311	7394.073	0.726334	10.17081
Standard Deviation	307.5648	2507.636	0.187925	1.954578

Figure 33: Picture of a failed specimen with the joint.

The results of the test show that the bamboo specimens with the joints are stiffer and stronger than the bamboo specimens without the joints but only slightly. The increased strength and stiffness is caused by the joint because the joints acts like a reinforcement ring on the bamboo. The bamboo material around the joint is stronger. The specimens without the joint fractured from end to end. A failed specimen is shown in figure 33. On the other hand, the specimens with the joints failed from joint to joint. This gives hint to the fact that the joints acted are a boundary and created a stress concentration at the joint. An example of the failed specimen with a joint is shown in figure 34.

Figure 34: Picture of a failed specimen without the joint

The specimen without the joint fractured in the manner seen in figure 34 in which a crack propagated from one end of the bamboo rod to the other end of the rod. The specimen with a joint fractured in a more catastrophic manner. The specimen in figure 33 is not intact because at the moment of fracture it exploded. Theses bamboo specimens fractured in this manner because of the enclosed boundary that was created by the joints. The energy had to be released in the normal direction of the rod because axially it was restricted by the enclosed joints.

Conclusion

This analysis shows the possibility of an electric-powered hover board without using a skirt. With today's technology, this is definitely feasible given the right amount of funds and supplies. If a hover board were to be developed using this analysis and current technology, the implications for usage span from military operations or cargo transport, to personal recreation or sports. While this project analyzes many aspects critical to proper operation and manufacturing of a hover board, this alone is not enough to develop one. The electrical system, a control system and a safety system would need to be further developed. This project, however, provides a solid foundation for any company with the time, money and technology.

The project starts with choosing a basic hover board configuration and starting to analyze the systems, and change accordingly. The structure is made entirely of carbon fiber sandwiching a Nomex honeycomb core and resembles a large skateboard. The internal structure is composed of 2 box beams to resist the load of a rider, the other components of the hover board, and the stresses caused by the propulsion system.

The propulsion system was narrowed down to two options: compressors and ducted fans. Compressors didn't prove to be practical due to the high complexity of such a system and the high power requirement. Ducted fans were chosen instead for their simplicity and high efficiency. Using Matlab and JavaProp, the ducted fans were sized and the propellers were optimized for the highest efficiency and highest thrust. To distribute the thrust across the length of the board and to distribute the stresses on each fan more evenly, four fans are used, each the same size. The duct was designed to be a constant area one because a converging nozzle requires more power.

The power required by the four fans will be provided by the Oxford electric motor, which is able to provide more than enough power for the system. Its low weight, small size and high power rating makes it the optimal choice for the power system. The current one that is developed will suffice for today's technology, but future advancements should make it even smaller, lighter, and more applicable to the hover board. The motor is powered by Lithium-Ion batteries, sized according to the project requirements. The overall weight is well within a reasonable weight allowance for the hover board.

Hover technology has already been used in many applications, but never in such a way as this project showed. This project shows that with today's technology, a non-skirted hover board is a possibility.

Acknowledgements

We would like to thank Dr. Elghandour for his guidance and support throughout this project. We would also like to thank Etuate Varea and Robert Jones for assisting us in completing this project.

References

[1]"Hovercraft History." *Links999. Man and Machine. Utopia.* Links999. Web. 08 June 2011. <http://www.links999.net/hovercraft/hovercraft_history.html>.

[2]"R/C Super Hovercraft,1:8 Radio Controlled Hovercraft,hovercraft China Wholesale." *China Trader Online - Wholesale Products from China - Professional Chinese Wholesaler*. CTO International. Web. 08 June 2011.

[3]Marshall, Andrew C. *Composite Basics.* Tabernash, CO: Aircraft Technical Book, 2007. Print.

[4]"Boeing 787 Dreamliner Maiden Voyage Ends With A Smooth Landing - Indyposted." *Indyposted - U.S. And International News*. IndyPosted. Web. 08 June 2011. <http://www.indyposted.com/7539/boeing-787-dreamliner-maiden-voyage/>.

[5] Dorworth, Louis C., Ginger L. Gardiner, and Greg M. Mellema. *Essentials of Advanced Composite Fabrication and Repair*. Newcastle, WA: Aviation Supplies & Academic, 2012. Print.

[6]"Unidirectional Carbon Fiber Sheets(Cloth)--12k (China Trading Company) - Other Construction Materials - Construction & Decoration Products." *DIYTrade - Largest China Product Directory,B2B Trading Platform with China Suppliers, Manufacturers. - DIYTrade China Manufacturers*. DIYTrade. Web. 05 June 2011. <http://www.diytrade.com/china/4/products/3094840/Unidirectional_Carbon_Fiber_Sheets_Cloth_-12k.html>.

[7]"Home Made Composites (HomMaCom) - What Are Composites ?" *Composite Materials Research at Ghent University - Mechanics of Composites*. Home Made Composites. Web. 30 May 2011.

[8] Jones, Robert M. *Mechanics of Composite Materials*. Philadelphia, PA: Taylor & Francis, 1999. Print.

[9]"What Are the Basic Types Bridge." Bigatoll.com. Web. 30 May 2011. <http://www.bigatoll.com/what_are_the_basic_types.html>.

[10]PARAMBIL, JITESH CHERUKKADU. *STRESS ANALYSIS OF LAMINATED COMPOSITE BEAM WITH I-SECTION*. Thesis. The University of Texas at Arlington, 2010. Arlington: Jitesh Cherukkadu Parambil, 2010. Print.

[11] Stejskal, Vaclav. "Composite Sandwich Core Panel - Machanics and Principals." *Wooden Kayak Designs by One Ocean Kayaks*. Wood Core Kayak. Web. 08 June 2011. <http://www.oneoceankayaks.com/Sandcore.htm>.

[12] Davis, Harmer Elmer, George Earl Troxell, and George F. W. Hauck. *The Testing of Engineering Materials*. New York: McGraw-Hill, 1982. Print.

[13] Hansen, J. "10.5.1.1 3-Point Bending Test." *Brevier Technical Ceramics*. Breviary. Web. 28 May 2011. <http://www.keramverband.de/brevier_engl/10/5/1/10_5_1_1.htm>.

[14]"Servohydraulic Fatigue Testing Machine." *Instron*. DirectIndustry. Web. 8 June 2011. <http://www.directindustry.com/prod/instron/servohydraulic-fatigue-testing-machines-18463-428354.html>.

[15]"Vacuum Bagging: Basics - Composite Materials." *Composites/Plastics*. The New York Times Company. Web. 08 June 2011. <http://composite.about.com/od/aboutcompositesplastics/l/aa000109.htm>.

[16]"Sikorsky Engine Nacelles." *RB Aero Building Blog*. RB Aero Building. Web. 08 June 2011. <http://blog.rbaeroplane.com/2009/09/19/sikorsky-engine-nacelles.aspx>.

[17] "Standard Test Method for Flexural Properties of Unreinforced and Reinforced Plastics and Electrical Insulating Materials by Four-Point Bending." *ASTM International*. American Society for Testing and Materials, 01 04 2011. Web. 1 Jun 2011.

[18] "Oxford YASA Motors axial flux motor yields monster Torque" Auto Green Magazine 2010. <http://autogreenmag.com/2010/09/30/oxford-yasa-motors-axial-flux-motor-yields-money-monster-torque/>